Atmospheric Research 281 (2023) 106493

Contents lists available at ScienceDirect

Atmospheric Research

journal homepage: www.elsevier.com/locate/atmosres

Galernas: A history of coastally trapped disturbances (2003–2020) with hidden frontogenesis in the Bay of Biscay

Gotzon Gangoiti *, Ana Rodríguez-García, Estibaliz Sáez de Cámara, Eduardo Torre-Pascual, María Carmen Gómez, Maite de Blas, José Antonio García, Estíbaliz García-Ruiz, Iñaki Zuazo, Verónica Valdenebro, Jon Iza

Faculty of Engineering, University of the Basque Country UPV/EHU, Bilbao, Spain

ARTICLE INFO

Keywords:
Coastally trapped disturbances
Galerna
Bay of Biscay
Frontogenesis
Mesofront

ABSTRACT

Galerna is the term accepted for an abrupt westerly change that affects the north coast of Spain. The wind surge travels from the mid-north coast of Spain to France, generally reaching their maximum intensity at the Basque Coast, and cuts off a period of hot weather, clear skies, and calm conditions at sea. The galernas have a large history of shipwrecks and fishermen deaths. They have been characterized as coastally trapped disturbances (CTD) and their propagation, enhanced with the local formation of a micro-front, was documented to behave like a density current. Alternatively, synoptic fronts have also been reported to cause galernas, considered to be more intense than those generated by a local micro-front. In this article we have generated the first climatology (2003–2020) of these events based on an objective identification methodology. The developed Event Identification Software (EIS), based on both 10-min surface station data and hourly ERA5 reanalysis fields, together with a new Front Identification Scheme (FIS) have enabled a deeper study into the origin and development of these micro-fronts, and a more comprehensive exploration of the interaction of the oceanic fronts entering the Bay of Biscay. Our results show that the area receives an average of four to five relatively intense galernas ($V_{max} > 50$ km h^{-1}) per year. Their number shows a great interannual variability (from one to seven) and a marked seasonality: May and June concentrate the largest fraction (almost one episode each year) and practically no episodes in winter. They occur more frequently between noon and the late afternoon, where the most intense wind records concentrate. Very strong galernas ($V_{max} > 72$ km h^{-1}) have occurred in all 18 years, can happen in any month from February to November, and their monthly distribution does not show the mentioned seasonality. On the contrary, the highest rates of temperature decrease across the galerna front in the coastal stations ($-\Delta T/0.5$ h > 4 °C) do have a stronger seasonality, with May and June concentrating a relatively large number of cases with a more abrupt temperature drop. The FIS shows that most of the galernas (83.5%) have a local origin inside the Bay of Biscay, and only a few ones (16.5%) are caused by oceanic fronts initiated out of the region. The local frontogenesis is more frequently initiated by the relatively cold marine southwesterly pre-frontals preceding a parent oceanic front and blowing against the warm continentals inside the Bay of Biscay, after being ducted along the north and northwestern coast of Spain. This hidden local frontogenesis, first revealed by the FIS, seems to be enhanced by the observed lee troughing, which could have both a thermal and dynamic origin, acting simultaneously after the intense Foehn at the coastal strip, preceding the formation of the galerna front. The local front enhancement appears to be the reason for the apparent jump of the primary front, which may eventually weaken, and even disappear, as the galerna front sharpens. Even during the more occasional frontal galernas, directly caused by the westerlies or north-westerlies behind the oceanic front, their eastward propagation is more rapid over the coastal area. The front deforms in shape and may cause its characteristic unexpected/abrupt irruption. All the EIS detected galernas, even the frontal ones, are wind reversals caused by a coastally trapped marine boundary layer. The upper-level ridge over Europe, observed in all of them, seems to be a synoptic ingredient for their development, preventing the eastward propagation of Atlantic depressions and enhancing at the same time the temperature and pressure gradients between the marine and continental air masses.

* Corresponding author at: Plaza Ingeniero Torres Quevedo, 1, 48013 Bilbao, Spain.
E-mail address: g.gangoiti@ehu.eus (G. Gangoiti).

https://doi.org/10.1016/j.atmosres.2022.106493
Received 15 July 2022; Received in revised form 6 October 2022; Accepted 26 October 2022
Available online 30 October 2022

1. Introduction

Following the definition of the Spanish Weather Agency (AEMET), a galerna is a sudden strong or very strong, and gusty wind, accompanied or not by precipitation, typical of the northern coast of Spain, and that abruptly cuts through a mild and generally hot weather. In France it is called galerne and "entrée maritime subite". Its sudden onset (gusty-squally character) and the rapid west-to-east propagation are its main features. The winds can reach ten-minute averages of 80 km h^{-1} with gusts above 100 km h^{-1}, but most of them do not reach such high values. The state of the sea also worsens rapidly. It always replaces surface warm and fair weather at the coastal strip, with continental easterly or southerly winds associated with Foehn in the lee of the coastal mountains, with an extremely gusty cold and humid gale-force marine north-westerly wind, running parallel to the coastal mountain range. The time span of the intense north-westerly winds (above 50 km h^{-1}) during a galerna is below 3–4 h, and most frequently under 1.5 h (AEMET, 2016; Gaztelumendi et al., 2011). The most intense gusts are reached rapidly (rarely takes more than an hour) after an abrupt temperature drop of 10–12 °C (Gaztelumendi et al., 2011; Aranda and Mader, 2012; Liria and Aranda, 2013). Its horizontal scale is 80–120 km cross-shore and 250–300 km along-shore at the easternmost region of the northern coast of Spain, while the vertical scale is below 1000–1500 m. Occasionally the leading edge of a galerna is marked by an arc cloud aligned almost perpendicular to the coast. However, precipitation is not usually associated with galernas, although it can occur sometimes.

The abruptness of the wind change makes galernas particularly hazardous. In Cantabria and in the Basque Country (BC), at the eastern region of the coast (Fig. 1), the word "galerna" is still associated with shipwrecks and death of fishermen, which occurred more often when the navigation was under sail, but the tragedies still remain in the collective memory of the seamen. Over the centuries the seamen sailing the Bay of Biscay (BB) from southern France to cape Finisterre (Fig. 1) in the north-western corner of Spain have feared the galerna because of its unexpected onset, its violence and the large number of shipwrecks and drownings associated with it. The list of severe storm years in the nineteenth century is very long (Casado, 2005), but the worse, named "Easter Saturday's galerna", occurred on 20 April 1878: in Santander 132 fishermen drowned, while a further 190 died from Bilbao to San Sebastián. In total, >320 fishermen died in a single afternoon and almost 500 crafts sank. Fishing crafts were since improved with a full deck, and both a weather forecasting service and a shipwreck rescue service began operating, but galernas on 1882, 1890, 1892, and 1908 were particularly bad. On 12 August 1912, 143 fishermen died, 116 of them from the same fishermen village of Bermeo, located in the Basque coast. The gradual introduction to the fishing fleet of the steam engine, first, the petrol-fueled engine later on, and the major improvements of the fishing boat designs greatly reduced the dangers of the galernas for ships and men. More recently, on 12 July 1961, 21 fishing boats sank and 83 fishermen died, while many boats suffered major damage. On 7 June 1987, eight people died with different type of accidents caused by wind during the galerna, most of them inland. Now the accidents are more related with recreational activities in beaches, small boating, sportive sailing, and tree falling in coastal areas. Flight operations near coastal airports can also be affected. Nowadays, the true nature of some of these maritime storms is still being discussed. That of July 1961 was caused by an explosive cyclogenesis of a depression in the NW limit of the BB. However, survivors described that the event was preceded by calm wind and sea conditions followed by a hard and sudden irruption. On that occasion, the intense winds and large waves lasted 3 days.

In the late eighties, the AEMET regional center in the Basque Country defined three types of galernas: frontal, typical (non-frontal), and hybrid. At the end of the 1990s, AEMET reduced them to two: those associated with frontal systems and non-frontal galernas (AEMET, 2018). Following the AEMET description, non-frontal galernas are generally less intense than frontal ones, they are more frequent in summer, and occur with no synoptic cold fronts whereas frontal galernas are more frequent in spring but also can happen in summer and even at the beginning of the fall season. Moreover, after a careful reading of the cited references one can assume that the key characteristics to

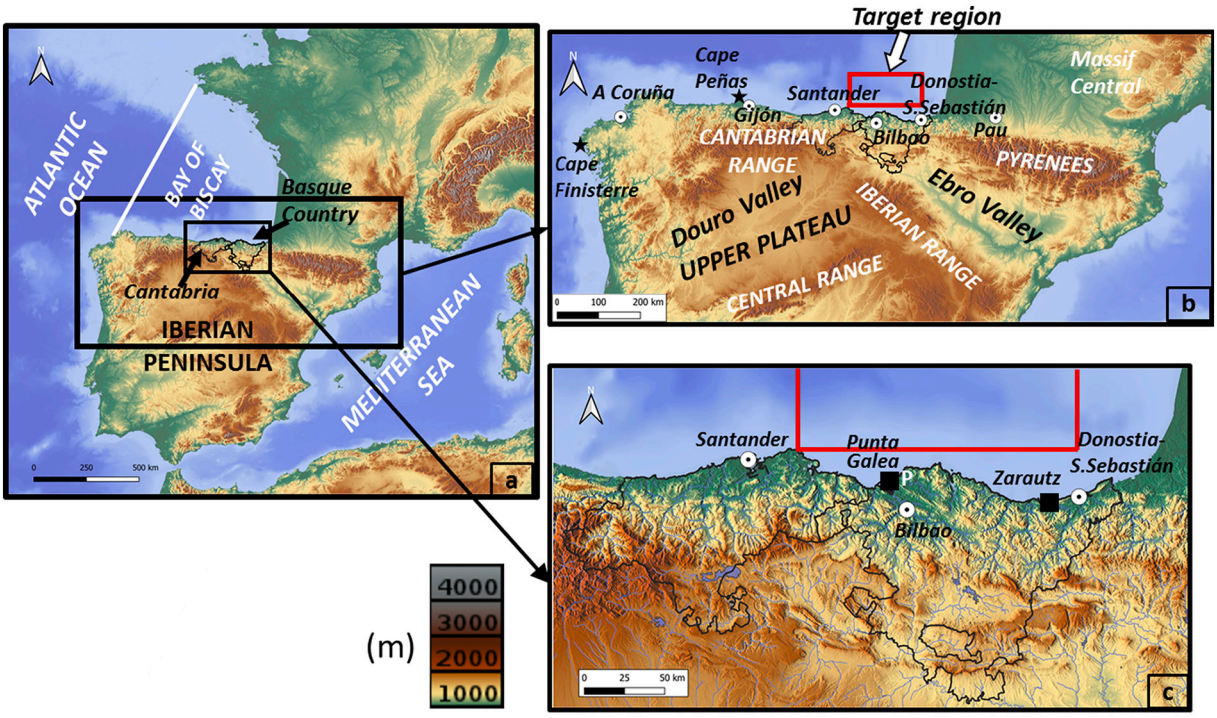

Fig. 1. Topography of (a) south-western Europe (Spain, Portugal and France), with (b) the location of (★) capes, (☉) urban sites, mountain ranges and valleys mentioned in the article. The (c) enlarged figure shows the location of (P) the WPR, (■) the meteorological surface stations and (red rectangle) the target area used for the identification of the galerna events. (For interpretation of the references to colour in this figure legend, the reader is referred to the web version of this article.)

distinguish a frontal galerna from the passage of a "classical" winter cold front seem to be: (1) the season of the year, out of winter, (2) more calm conditions or weaker-warmer southwesterly pre-frontals preceding the irruption of the galerna, and (3) a shorter duration, 45–90 min, of the north-westerlies behind the cold front (AEMET, 2018; AEMET, 2016).

Different attempts have been made to understand the onset of galernas and to arrive to their correct forecasting, but we have not found a climatology of these events with an objective identification of episodes. Arasti (1999, 2001), after the analysis of a case study of a non-frontal galerna occurred on 25 July 1995, described its onset and development due to"the presence of a synoptically driven alongshore pressure gradient, which was amplified by a mesoscale tendency of increasing pressures at the western region and a simultaneous decrease in the eastern margin of the coastal strip". In these contributions, the observed tendency is associated with the simultaneous cold and warm advection of air at the western and eastern regions, respectively, of the northern coast of Spain. During this strong event, pressure and temperature gradients as well as alongshore wind intensity increased from west to east and a micro-front formed and intensified while it moved parallel to the coast. Pressure and temperature gradients of 5 hPa in 50 km and 13 °C in 30 km, respectively, were observed, with wind velocities over 25 m s^{-1} at the Basque coastal area (eastern region), where the galerna reached the greatest intensity. This study states that the galerna event starts with the cold advection from the west, it shows a considerable vertical wind shear, and its depth is usually <1000–1500 m ASL. As recorded by the Wind Profiler Radar (WPR) by Euskalmet (Basque Service of Meteorology), located at point P in Fig. 1c, southerly and warm offshore winds blow on top, whereas onshore marine north-westerlies blow (or "do it") at the surface. The author showed that, at least at its final stage (before crossing the coast of France), the observed case of a strong, non-frontal galerna behaved like a density current moving at increasing propagation speed from Santander (14 m s^{-1}) to San Sebastián (20 m s^{-1}) in the target region of Fig. 1, where the maximum intensity is reached.

The non-frontal galernas have been identified (Arasti, 1999) as Coastally Trapped Disturbances (CTD). A CTD can be defined as a "marine-layer air flow that is rotationally trapped (Coriolis force) against the coastal mountains and vertically by stable stratification, such that it can propagate with the topography on the right (left) in the Northern (Southern) hemisphere, following an alongshore pressure gradient". Typical CTD length-scales, as described in the bibliography, are of the order of 1000 km alongshore and 100–300 km cross-shore (Reason and Steyn, 1990). They have a time span of 2 to 6 days and usually cause important changes to the local coastal weather with dry and clear sky conditions being replaced by coastal stratus or fog. Drizzle may also occur, and winds reverse direction and strengthen while the system propagates through. CTD have been studied in many regions worldwide such as in South Africa (Gill, 1977; Reason and Jury, 1990), the Pacific coast of North America (Mass and Albright, 1987; Nuss et al., 2000; Rahn and Parish, 2008; Parish et al., 2015) where they are also called coastally trapped wind reversals (CTWR), and southeastern Australia (Colquhoun et al., 1985; Reid and Leslie, 1999; Wang et al., 2020), among other locations. More recently, González et al. (2018), described a coastally trapped disturbance initiated by Tramontane winds in the north coast of Catalonia, in Spain, as a density current front, with a length scale and time span more similar to the galerna. In this later contribution, as well as in the case of the CTDs of the SE coast of Australia (Wang et al., 2020; Australian Government Bureau of Meteorology, 2011), synoptic fronts were shown to initiate the documented surges. This should also be the case for the so-called frontal galernas as discussed in the next sections.

There are no documented studies about the temporal variability of galernas, seasonal preference, possible inter-annual trends, and main statistics of episodes, with average and extreme cases. Thus, a first objective of this article is to generate a climatology of these wind surges by using an objective identification methodology based on the 10-min time resolution of local surface station data, together with the hourly ERA5 reanalysis on pressure levels (Hersbach et al., 2020; Copernicus Climate Change Service, 2018). The second objective is to explore the frontal systems associated with the origin of these episodes and to deepen in both their propagation and dynamics. For this later objective, a methodology will be set up to draw and track the fronts, based on the high-resolution hourly ERA5 reanalysis wind field. Front tracking is the critical step to identify frontal structures accompanying the galerna development. Consequently, the adequacy of the current classification of frontal and local non-frontal galernas, with their respective synoptic scale and micro-fronts, can also be explored. The 6-hourly ERA-Interim reanalysis time-resolution is not adequate to assess a meteorological process that usually takes <3–4 h to complete, such as a galerna event.

The paper is organized as follows: section 2 is devoted to the area description, including the topography and the location of the selected meteorological stations. The methodology is also included in this section: the algorithm designed for the objective identification of galernas is described as well as the set of algorithms proposed for the frontal depiction based on the hourly ERA5 reanalysis. In section 3, the origin and evolution of two galernas are discussed after the observed changes in the revealed frontal depiction and its propagation. The climatology (episode identification) of galernas during the 18-year period 2003–2020 is described in section 4, together with a sensitivity analysis to the parameters used in the identification algorithm. Section 5 shows the average and anomalies of the synoptic meteorology during galerna events, and the main conclusions are summarized in section 6.

2. Area description and methodology

2.1. Area description

The topography of northern Spain is characterized by the presence of two major mountain ranges, the Cantabrian Range (highest peaks between 2000 and 2600 m) and the Pyrenees (2000–3500 m), both with steep mountains and deep valleys (Fig. 1). The Basque Country, located in the north-centre between these two main mountain ranges, forms a gap between the Pyrenees and the Cantabrian Range, with a group of smaller mountains (highest peaks between 1000 and 1500 m) and populated narrow valleys. The long coastal strip from cape Finisterre to southern France adds land–sea interactions to the local weather of northern Spain, clearly influenced by marine advections, which conditions its climate. The coastal strip of the Atlantic slope, very rainy with moderate temperatures softened by the influence of the sea, hosts the main urban areas, from West to East (Fig. 1): A Coruña, Gijón, Santander, Bilbao and Donostia-San Sebastián. The climate of the coastal valleys and mountains facing the sea can be classified as Cfb following the Köpen-Geiger climate classification. The mountain barriers are responsible for a rapid transition from the maritime weather at the northern coast to the more continental of the inner landmass of the Iberian Peninsula: the Douro valley in the upper Iberian plateau and, to a less extent, the Ebro valley are sheltered from the mild and humid oceanic air mass intrusions, and show a high degree of continentality. On the contrary, the lower lands of the south-western coast of France allow for a deeper inflow West-to-East of the marine air masses into the continental landmass to the North of the Pyrenees. As a result, the oceanic influence in southern France extends further eastwards from the Atlantic coast into the western Massif Central (Fig. 1).

Fig. 1 also shows the location of the selected meteorological surface stations (Punta Galea and Zarautz) of Euskalmet and its WPR (P in Fig. 1c), located on top of a 60-m-high cliff directly over the sea (Punta Galea). The site is on the right bank of an estuary that runs nearly 16 km from the city of Bilbao to the coast. The main characteristics of the WPR at Punta Galea have been described in detail by Alonso et al. (1998). The system (LAP 3000 at 1290 MHz) is mounted with nine antenna panels. Its operation includes signal processing on five beams and two pulse widths (100 - and 400 m vertical resolutions). Hourly or half-hourly

wind averages were obtained continuously every day with a total coverage of 24 h per day and a variable vertical coverage between 3000 and 5000 m. It started operating in 1996 and it helped to understand the internal wind structure and vertical coverage of galernas (Arasti, 2001; Gangoiti, 2002, 2003), among other severe weather episodes (Gangoiti et al., 2000; Gangoiti et al., 2002). After prolonged down periods due to breakdowns, maintenance, and repair work, it stopped working in 2015.

2.2. Event identification

In order to produce a climatology of galernas using an objective identification of these episodes we have used the hourly ERA5 reanalysis together with the 10-minute time resolution data of two surface stations of Euskalmet. The meteorology produced by this Service is open-access with data recorded since 2003, available from all the stations in the Basque Country (https://euskalmet.beta.euskadi.eus/s07-5853x/es/meteorologia/datos/mapaesta.apl?e=5). Two stations at the coastal strip (Punta Galea and Zarautz), shown in Fig. 1, have been selected to design the algorithm for the identification of episodes. The total time span included in this study is 18 years (2003–2020). The network of automatic stations is well maintained. We have found a low number of missing and suspect data values in the referred stations along the years, with a typical coverage close to 98%–99% of data in both stations. Exceptionally, the lowest annual coverage (93.4%) corresponded to station Zarautz during the year 2007. Missing and suspect values were replaced with a simple linear time-interpolation, which was effective to avoid temperature and wind velocity abrupt changes, which could be interpreted as false positive galerna identifications. However, the gaps could have occurred during periods with galerna events; thus, the number of identified events could be higher.

The designed Event Identification Software (EIS) is based on a series of conditions, which must be jointly met to accept a positive recognition. The imposed conditions try to substantiate the observations-descriptions of the galernas mentioned in the bibliography (section 1). They include: (1) a lower limit of the rate of temperature decrease, (2) wind gusts above a critical value, after the temperature drop, (3) sustained north-westerly winds during a period after the temperature drop, with (4) an intensity above a reference value, and (5) a net wind increase across the temperature drop. This last condition is in line with the preceding weaker pre-frontal south-westerlies during a galerna event at surface level (AEMET, 2018). All these requirements have to be fulfilled for both stations, Punta Galea and Zarautz, with a maximum time lag of 3–4 h between their respective temperature drops, which always have to occur first at Punta Galea. The distance between these stations is 72 km, and most of the documented galerna episodes (Arasti, 2001; Gaztelumendi et al., 2011; Liria and Aranda, 2013; Aranda and Mader, 2012) covered the distance in <3–4 h, and typically in <1.5 h. Fig. 2 shows the time variation of various meteorological parameters during three galerna events on 4 March 2007, 31 August 2009, and 4 June 2015. The first two, analyzed in section 3, are included in a list of 17 (relevant) galernas between 2001 and 2011 recorded by Gaztelumendi et al. (2011). The last one is a more recent event, and all three have been identified by the EIS (section 4). The time instant of the maximum recorded temperature drop (vertical line in all panels) is concurrent with a wind shift, a

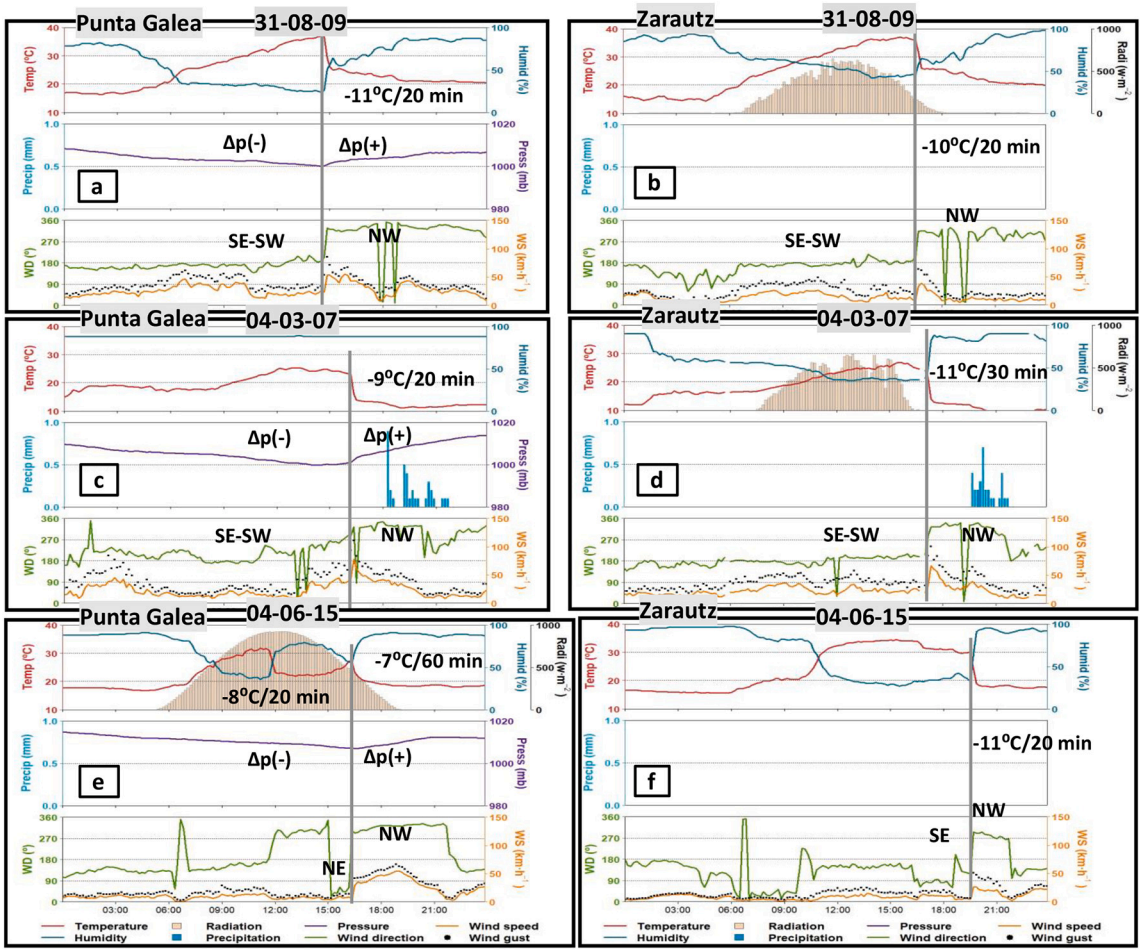

Fig. 2. Time variation of various meteorological parameters during three galerna events on (a-b) 31 August 2009, (c-d) 4 March 2007, and (e-f) 4 June 2015 at the Punta Galea (left) and Zarautz (right) EUSKALMET stations in the Basque coast: temperature, relative humidity, pressure, precipitation, wind speed, direction and wind gust (black dots) from 10 min observations are represented when available.

pressure increase (+Δp), humidity increase, occasional precipitation (4 March 2007) and a wind increase, with a maximum that sometimes is delayed after the main temperature drop, as in (e) 4 June 2015 at Punta Galea. As observed in the Figure, there is a great variety in the galerna wind and temperature records: the wind can increase abruptly after the temperature drop, as for the first two cases, or do it more progressively during a time lapse of up to 3–4 h, like on 4 June 2015 at Punta Galea, when the wind surge was more abrupt at Zarautz. During the same case study, the temperature drop at Punta Galea was weak (7 °C in 1 h), probably because it had recorded a previous sea breeze near noon, with the associated wind change and temperature decrease. However, this was not the case for Zarautz, where a strong temperature drop with no previous sea breeze was registered. In order to cope with the observed variety of cases we have selected a series of initial limits for the wind and temperature records (reference selection). These parameters follow the observed values of a series of identified galerna events (frontal and "non-frontal") in the available bibliography (Arasti, 1999, 2001; Gangoiti, 2002, 2003; Gaztelumendi et al., 2011). Section 4 will show a sensitivity analysis of the designed algorithm to changes in the prescribed limits, as well as its verification against previously recorded galerna cases. The prescribed set of parameters of the reference selection is:

1) $-\Delta T/1\ h > 4\ ^{\circ}C$.
2) $V_{max} > 50\ km\ h^{-1}$.
3) $260 < Dir_{1h} < 360$.
4) $V_{1h} > 50\ km\ h^{-1}$.
5) $\Delta V > 0\ m\ s^{-1}$.

Where,

$-\Delta T/1\ h$ = rate of the temperature decreases in a time lapse of 1 h,

V_{max} = wind gust maximum of the galerna, evaluated during a time span of 4 h after the temperature drop ($-\Delta T/1\ h > 4\ ^{\circ}C$), in line with the observed time scales.

Dir_{1h} = 1-hour average of the wind direction, after the V_{max} gust occurrence,

V_{1h} = 1-hour average of the wind speed, after the V_{max} gust occurrence, and.

ΔV = wind intensity changes across the temperature drop ($-\Delta T/1$ h): $\Delta V = V_{1h} - V_{1h\_b}$, where V_{1h_b} is the 1-hour average wind speed before the temperature drop.

The referred conditions must be jointly satisfied in both stations, but we have allowed the wind velocity criteria V_{max} to be fulfilled only in one of the two stations. In order to enable the review and further analysis of the results we have recorded the wind data and remaining parameters ($\Delta T/1$ h, V_{max}, V_{1h}, ΔV, Dir_{1h}) of both stations after the identification of each galerna event. Similar temperature and wind limits, at selected surface stations, are used for the identification of Tramontane surges in NE Spain (González et al., 2018) and the "Southerly Busters" of SE Australia (Australian Government Bureau of Meteorology, 2011): wind gusts over 54 km h^{-1} and temperature decrease $-\Delta T/3$ h over 5 °C are used in the latter case, while similar wind gusts of 50 km h^{-1} and wind direction limits in two surface stations are used in the Tramontana surges.

The hourly ERA5 reanalysis data on pressure levels are used to include in the algorithm the required stability criteria of the Marine Boundary Layer (MBL) behind a CTD, as described by Arasti (1999, 2001). The following parameters (6, 7) are estimated inside the target region (rectangle) drawn in Fig. 1b and c (between longitude 3.5^0 W – 2^0 W and latitude 43.5^0 N – 44^0 N), after the detection of the wind shift in the region:

6) $Fr_m < 1$.
7) $WS > 0$.

Where,

Fr_m = mountain Froude in the target area, $Fr_m = \frac{V_{1000}}{h_m N}$,

h_m = mountain range characteristic height at the coastal strip (1200 m),

V_{1000} = average wind intensity inside the target area at 1000 hPa pressure level,

N = Brunt-Väisälä frequency (s^{-1}), $N = \left[\frac{g}{\theta}\frac{\Delta\theta}{\Delta z}\right]^{\frac{1}{2}}$

g = gravitational acceleration, 9.81 m s^{-2},

θ = area averaged ambient potential temperature at 1000 hPa,

$\Delta\theta/\Delta z$ = vertical gradient of the ambient potential temperature in the MBL (between 1000 hPa and 850 hPa),

WS = vertical Wind Shear in the target area, $WS = \frac{\left|\vec{V}_{800} - \vec{V}_{1000}\right| \cdot (v_{800} - v_{1000})}{|v_{800} - v_{1000}|}$,

v_{800} = Eulerian N-S wind component at 800 hPa,

v_{1000} = Eulerian N-S wind component at 1000 hPa, and

$\left|\vec{V}_{800} - \vec{V}_{1000}\right|$ = modulus of the difference between the averaged wind vectors at 800 hPa and 1000 hPa inside the target, $+\sqrt{(u_{800} - u_{1000})^2 + (v_{800} - v_{1000})^2}$

u_{800} = Eulerian *E*-W wind component at 800 hPa,

u_{1000} = Eulerian E-W wind component at 1000 hPa

Both wind and temperature variables were evaluated at the time of the maximum northwestern (315^0) ERA5 wind component intensity of the 1000 hPa winds inside the target within the first three hours since the wind shift. This is intended to capture the time when the air mass behind the galerna front spreads throughout the target region.

Backing winds (WS > 0), turning counter-clockwise with height with the offshore south-westerlies blowing above the mountain crests and the marine north-westerlies at the coastal strip, are a well-known feature of the galernas, with a marine layer decoupled from the upper-level winds. This is not the case during the more frequent marine north-westerlies of the cold season, when the winds at the lower levels of the coastal strip follow the coastal geometry or alternatively are directly channeled into the main estuaries of the coastal valleys, while at upper levels the synoptic northwesterly forcing can flow over the coastal barrier. Consequently, WS could be negative (wind veering with height) or have low positive WS values whereas during a galerna event WS is always positive.

The mountain Froude Fr_m is a non-dimensional number that provides a measure of the relative importance of kinetic and potential energy in flow around and over obstacles when it is directed into them. If the Froude number is high (> 1), the flow is unblocked and the air will move freely over the obstacle (mountains); when it is low, the flow is around the obstacles (National Research Council, 1992). Low Fr_m conditions prevent the escape of energy upwards and high/low pressures generated in the region can duct the flow in the along-shore direction parallel to the barrier while the Coriolis force trap energy against the mountains that borders the northern coast. It is not necessary to have a blocked onshore flow for the orography to influence coastal winds. High-low pressure fields along the coast can generate a trapped flow and propagate along the coastline. With typical Brunt-Väisälä frequency (N) values between 0.01 and 0.1 of the MBL stratification, registered by the EIS for the reference selection (section 4), an elevation of 500 m is sufficient to cause blocking of the coastal surface winds in a range between 5 m s^{-1} and 50 m s^{-1}. As the estimated magnitude of the Fr_m number is highly dependent of the characteristic mountain height, wind, temperature, and pressure level selection, we have also included, in section 4, a sensitivity analysis of the EIS algorithm to changes in the prescribed Fr_m limits with respect to the reference selection.

The EIS, written using the GrADS scripting language (Doty and Kinter III, 1995), processes sequentially both the 10-min wind and temperature records of the two surface stations and the hourly ERA5 reanalysis temperature and pressure values inside the target area. Each positive identification is recorded as a line output, with the time and

main meteorological data of the event in both stations as well as the Brunt-Väisälä frequency, mountain Froude, and vertical wind shear in the target region, among other parameters.

2.3. Frontal identification

Both frontal and non-frontal galerna events have been described (section 1) as a specific type of synoptic or sub-synoptic frontal events. In addition, one of the bizarre features of these fronts are their rapid development and "unexpected" and abrupt irruption in the target area defined in section 2.1. Modern reanalysis products offer the opportunity of identifying and tracking midlatitude mobile fronts, which could be of great interest to achieve a deeper understanding of the origin and development of the different types of galernas. The results of the exploration will depend to some extent on the time and space resolution of the selected reanalysis product. Simmonds et al. (2012) developed an objective scheme for frontal identification in the Southern Hemisphere using the 6-hourly ERA-Interim reanalysis data. Unlike other schemes, which use thermal criteria (Hewson, 1998; Berry et al., 2011), their frontal tracking scheme uses only wind-related criteria to identify cold fronts. The system requires that both the wind shifts from the northwest to the southwest quadrant between sequential 6-hourly analyses and the change in the (signed) meridional wind component exceeds 2 m s^{-1} between consecutive analyses. The scheme has been shown to perform well compared to others, such as the one using the thermal criteria (Schemm et al., 2015). The latter has difficulties identifying fronts in areas of high temperature contrasts, such as coastal areas and regions with elevated topography, as it is the case for the northern coast of Spain. More recently, Bitsa et al. (2019) have used a modified version of the scheme by Simmonds et al. (2012) in the Mediterranean region, based as well in the 6-hourly ERA-Interim reanalysis on a $0.5^0 \times 0.5^0$ latitude-longitude resolution.

Hourly ERA5 reanalysis on a $0.25^0 \times 0.25^0$ latitude-longitude resolution were first available in 2018. This higher time (and space) resolution seems to be more adequate to track the sub-synoptic fronts associated with galerna events, with a characteristic lifetime of 3–4 h, as described in section 1. The GrADS scripting language has also been used here to build up our Front Identification Scheme (FIS), using the same meridional wind threshold component increase of 2 m s^{-1} suggested by Simmonds et al. (2012) which was useful for identification of oceanic cold fronts in the Southern Hemisphere. This time, the software is designed to spot wind shifts from the southwest to the northwest quadrant, using a variant of the above-mentioned threshold of the northerly component increase between consecutive wind fields separated by two hours. Previously, different tests were performed using other wind shift thresholds and time lapses from 1-to-4 h between subsequent wind fields. The results were compared with the 6-hourly surface analyses charts produced by the UK Met Office (https://www2.wetter3.de/) and the satellite images from the NOOA's Global International Satellite Cloud Climatology Project (ISCCP) B1 Browse System (GIBBS), available from https://www.ncdc.noaa.gov/gibbs/year (Knapp, 2008), used for validation. Our final selection of the wind shift threshold (2 m s^{-1}) and the time lapse between consecutive analysis (2 h) resulted both in a less "noisy" depiction of fronts (Gangoiti et al., 2022a) and a broad enough track of the wind shift region representing the frontal propagation. The left boundary of the wind shift area would correspond to the more recent (first hour) eastward propagation, and it could be assigned to the frontal position at the initial time of the sequential comparison. For the wind shift threshold we have tested values between 1 and 4 ms^{-1} and while the lower ones (1–2 ms^{-1}) keep the integrity of most of the oceanic fronts, the performance of the largest threshold (4 ms^{-1}) shows an excessive filtration of the fronts. Some of them look segmented and others simply disappear. For instance, on 4 March 2007, at 00 UTC the westernmost Atlantic front discussed in section 3.2 (front "a") is more fragmented when using the 4 ms^{-1} threshold value (Gangoiti et al., 2022b), while for the lowest velocity thresholds it shows a more continuous wind shift region, extending north-to-south at longitude 20 ^{0} W. At the same time, in the Mediterranean Sea using the lower thresholds (1–2 ms^{-1}), the FIS represents a Tramontana front (north of the Balearic Islands), which can be tracked for the following 4 h (Gangoiti et al., 2022b) and it can be related with the cloud bands of low-level clouds in the Meteosat IR image in section 3.2. This front is not represented in the synoptic surface charts and it can be removed by using the largest (4 ms^{-1}) threshold. Consequently, the FIS applied to the ERA5 wind fields with low velocity thresholds (1–2 ms^{-1}) seems to be more appropriate to detect mesoscale fronts, also keeping the integrity of the large synoptic fronts. This is also the case of the non-frontal galernas on 31 August 2009 and 4 June 2015, mentioned in section 2.2, where the lower thresholds show a better representation of the galerna mesofronts inside the BB region than the largest one (Gangoiti et al., 2022b). These types of fronts are absent on the synoptics scale surface pressure charts, and obviously cannot be used to validate their detection. Small wind shift regions without a coherent frontal structure, which disappear in consecutive hourly wind fields, are most frequently located on land and in regions of weak winds at sea, as shown in the temporal sequence of the fronts in the three case studies presented in (Gangoiti et al., 2022b). The largest threshold (4 ms^{-1}) can filter out these regions better that using the smaller threshold values, but at the expense of removing the real fronts. Other wind thresholds could be more appropriate in the identification of wind shift regions when using the 6-hourly ERA-Interim reanalysis for synoptic front detection (Bitsa et al., 2019) and filtering of erroneous fronts.

Warm continental easterlies over the BB can also precede the cooler marine westerlies during a galerna. Consequently, and with the aim of locating East-to-West wind changes that occur within the Bay during these events, we extended the original front tracking method of the Simmonds' technique. The developed software can also track east-to-west wind shifts using a similar 2 m s^{-1} threshold increase, this time for the zonal wind component of consecutive wind fields separated by two hours. Both types of wind shifts, east-to-west and southwest-to-northwest, can occur simultaneously inside the BB, where the continental easterlies from France and the prefrontal southerlies from the Iberian Peninsula can face the westerlies, creating the galerna fronts (section 3). The front tracking ability of the algorithm and its performance during the galerna events is shown in section 3 and 4.

3. Analysis of two case-studies

In order to show the observed frontal propagation during the galerna events, we present a detailed analysis of a selection of two case studies, previously identified by Gaztelumendi et al. (2011), which represent the two types of galernas described in the bibliography (section 1). The first one, on 31 August 2009, represents a non-frontal galerna (without a synoptic front), whereas the second, on 4 March 2007, is a frontal one. Their respective representativeness is discussed in section 4. The time variations of the meteorological variables recorded in the surface stations of Punta Galea and Zarautz during these two events have been reported in section 2.2.

3.1. The case-study of 31 August 2009 (non-frontal galerna)

Following the NOAA NCEP Climate Forecast System Reanalysis (CFSR) (Saha et al., 2014), the synoptic conditions on 31 August 2009 (Fig. 3a and b) are characterized by a large upper-level trough, which extends North-to-South from Iceland through the western coast of the British Islands and to the west of the Iberian Peninsula. This leaves the Azores High relocated further West than its average place in summer (Millán et al., 1997; Gangoiti et al., 2001) and a high-pressure area to the East over the European continental area, under an elongated upper-level ridge. Both surface high-pressure areas extend to the south, reaching the Atlantic coast of northern Africa to the west and down to the Mediterranean Sea to the East. These synoptic conditions force relatively warm

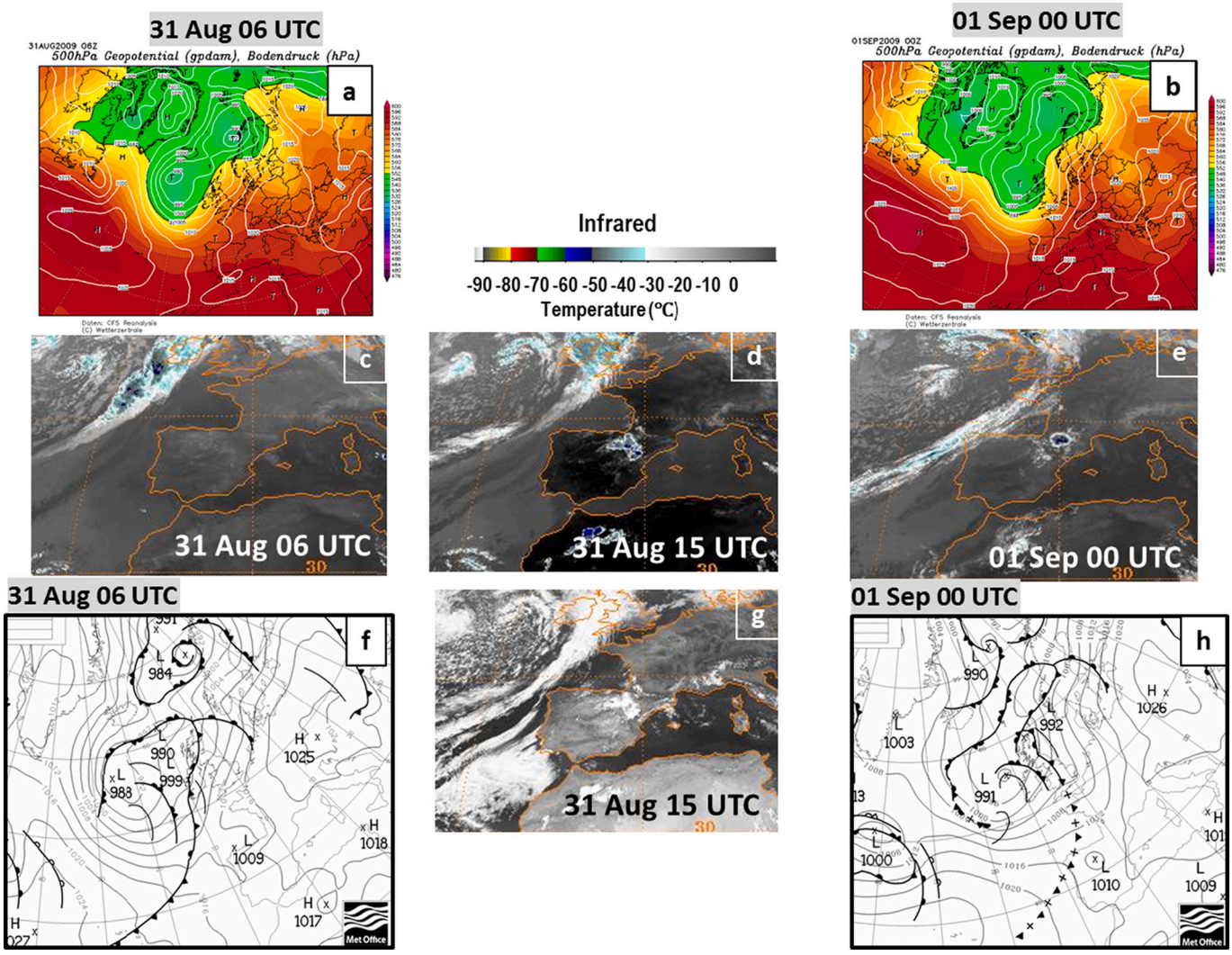

Fig. 3. Synoptic conditions during the galerna of 31 August 2009: 500 hPa geopotential heights (gpdams) in shaded colors and mean sea level pressure (MSLP) in contours at (a) 06 UTC and (b) 00 UTC of the following day (01 September), obtained from the Climate Forecast System Reanalysis (source: https://www.wetterzentrale.de). (c, d, e) Meteosat satellite IR and (g) VIS images (source: GIBBS imagery by NOAA) and (f, h) surface analyses charts produced by the UK Met Office (source: https://www2.wetter3.de/). The galerna crosses the Punta Galea station at 15 UTC and no synoptic front is detected at that point.

south-westerlies over northwestern Iberia and the BB at upper levels, which seems to intensify along the day following the increased gradients of the 500 hPa geopotential height over the region (Fig. 3a and b). Simultaneously, low Mean Sea Level Pressure (MSLP) gradients in the BB (Fig. 3a, b, f, h) are compatible with weak winds at surface level (Fig. 3f and h). However, the observed warm and dry southerlies (Fig. 2a and b) are relatively strong (6–8 m s^{-1}) with 14 m s^{-1} wind gusts in both selected coastal stations of the BC during the early morning and afternoon before the frontal passage (15 UTC) through the Punta Galea station (Fig. 2a). The analysis charts of the Met Office (Fig. 3f and h) show no frontal passage through the northern coast of Iberia. An Atlantic front, initially located at 06 UTC offshore, far to the west, is drawn weakened at the western edge of the north coast at 00 UTC of the following day. Eight hours before (at around 16 UTC) the front of a strong galerna (wind gusts of 24 m s^{-1}) has crossed to southern France. Meteosat satellite VIS and IR images (NOOA's GIBBS) in Fig. 3 show no evidence of the formation and development of the galerna. Convective clouds over the Ebro valley and the Iberian range, at 15 UTC in Fig. 3d and g, have no relationship with the galerna: they are the result of the convergence of the pre-frontal south-westerlies crossing the Iberian Peninsula with the combined sea-breeze and anabatic winds from the Mediterranean, following the Ebro valley.

The mentioned Atlantic front, shown in the satellite images and in the surface charts, is shown in blue in Fig. 4a (large domain g1), approaching to the northwestern corner of Iberia at 10 UTC. The blue shading represents ERA5 1000 hPa wind shifts from the southwest to the northwest quadrant, estimated by the FIS in m s^{-1} above the threshold value of 2 m s^{-1} (section 2). The alternative East-to-West wind shifts are shown in red. The Atlantic front position (in blue) at the latitude 43.5^0 N of the northern coast of Iberia is located at 14^0 W in the same Fig. 4a. In Fig. 4c (small domain g2), the galerna meso-front can be identified at the left boundary of the blue track at longitude 6^0 W of the coastal line, with a large area of *E*-W wind shift (in red), which crosses the complete BB up to the region of Brittany in the domain g1. The observed red and blue tracks preceding the parent Atlantic front separates the pre-frontal south-westerlies and the continental south-easterlies blowing on the BB. For this event, the initial detection of the galerna front by the FIS is at 06 UTC in the western corner of the coast (longitude 8.5^0 W), when the parent oceanic front is still offshore at 16^0 W, at a distance of around 600 km (Gangoiti et al., 2022a). The relatively cold oceanic pre-frontal MBL, topped by a temperature inversion between 600 and 1000 m ASL (profile 2 in Fig. 5d), is channeled around the coast of Galicia and then along the northern coast. The flow in the shallow MBL seems to be blocked on the western side of the coastal mountain ranges in Galicia

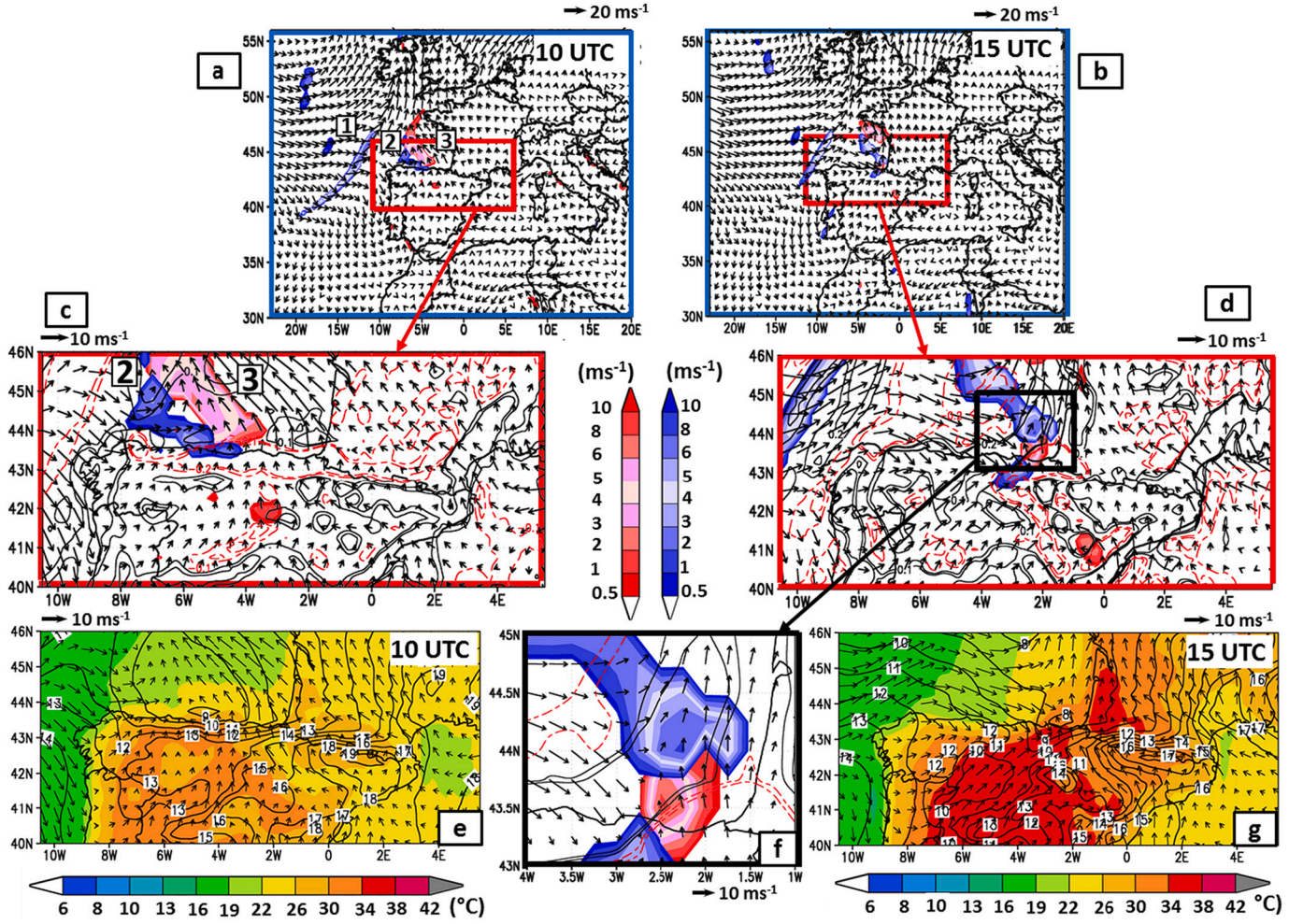

Fig. 4. ERA5 1000 hPa wind vectors and fronts on 31 August 2009: wind shifts (red and blue tracks) estimated by the Frontal Identification Scheme (FIS) for the large domain, (a) at 10 UTC, before the arrival of the galerna at the surface stations (b) at 1500 UTC, when it is detected at the Punta Galea surface station. The enlarged views (c and d), represent wind shifts and vertical wind speeds ($Pa \cdot s^{-1}$) in dashed red (sinking) and solid black (ascent) contours at the 950 hPa pressure level. In the bottom panels, the mean sea level pressure (MSLP-1000 hPa) in contours, the potential temperature (°C) in shaded colors and the 10-m wind vectors are represented for the same time instants. Panel (f) shows a detailed plant view of the galerna mesofront while crossing the target area. (For interpretation of the references to colour in this figure legend, the reader is referred to the web version of this article.)

(Fig. 4c and d), and diverges both to the south and to the east channeled by the coast of Portugal and northern Spain, respectively. Once inside the BB, the anticyclonic turning of the wind seems to be a response to the local pressure gradients developed between the marine cold advection and the warm continentals blowing ahead, which are dynamically heated by the intense Foehn in the lee of the coastal mountains of northern Spain (dashed red contours in Fig. 4c). The cold advection creates a ridge of relatively high pressure behind the galerna front (Fig. 4e). Simultaneously, troughing at the eastern side of the coast is enhanced by the evolution of the thermal low, which is advected over the BB by the warm continental southerlies blowing ahead of the galerna front, as shown in Fig. 4e and g. Winds behind the front do not reach the geostrophic balance as they progress along the coast and face increasing pressure and temperature gradients from West to East. At 15 UTC the meso-front is crossing the Punta Galea station (Figs. 2 and 4f). At this time, a large area of compensatory sinking is observed on the sea at the rear of the front (dashed red line in Fig. 4d), while a strong ascent is shown both at the leading edge of the galerna front and at the windward slope of the mountains to the right of the advancing shallow pre-frontal MBL (Fig. 4f and d).

The vertical sections of wind and potential temperature during the propagation of the galerna front are shown in Fig. 5. The three air masses (1-to-3) concerned in the development of the meso-front are represented in Fig. 5a (also shown in Fig. 4a) and they can be defined as (1) oceanic frontal (located behind the parent front), (2) oceanic pre-frontal, and (3) continental (modified over the BB). The described galerna front has developed directly inside the BB, between the oceanic pre-frontals (2) and the continental winds (3), far away from the parent oceanic front. Differences among the three air masses can be appreciated in the vertical profiles 1-to-3 (Fig. 5d) of the ERA5 potential temperature and specific humidity at three locations inside each air mass at latitude 43.5^0 N. This is assumed to represent the latitude of the coastal strip of northern Iberia (Fig. 5a). The three profiles, at longitudes 15^0 W, 10^0 W, and 3^0 W, are also represented with solid white vertical lines in Fig. 5e. The relatively cool ocean temperature is conditioning the lower temperature of the MBL inside the air masses 1 and 2 (Fig. 5d), which show similar values at the surface, while the continental air mass 3, with the southerlies blowing at all levels, show much higher temperatures and a very shallow, cool, and stable MBL (0–500 m) on the sea. This point 3 is located offshore, near the Punta Galea station, and shows a developing cool MBL topped by a quasi-adiabatic and well-mixed (constant specific humidity) air layer, which contains the continental warmer southerlies, preceding the galerna front.

The constant latitude 43.5^0 N cross sections along the northern coast of Iberia (Fig. 5e and f) show the progress of both oceanic and galerna fronts between 10 UTC and 15 UTC. At the bottom of these figures, the

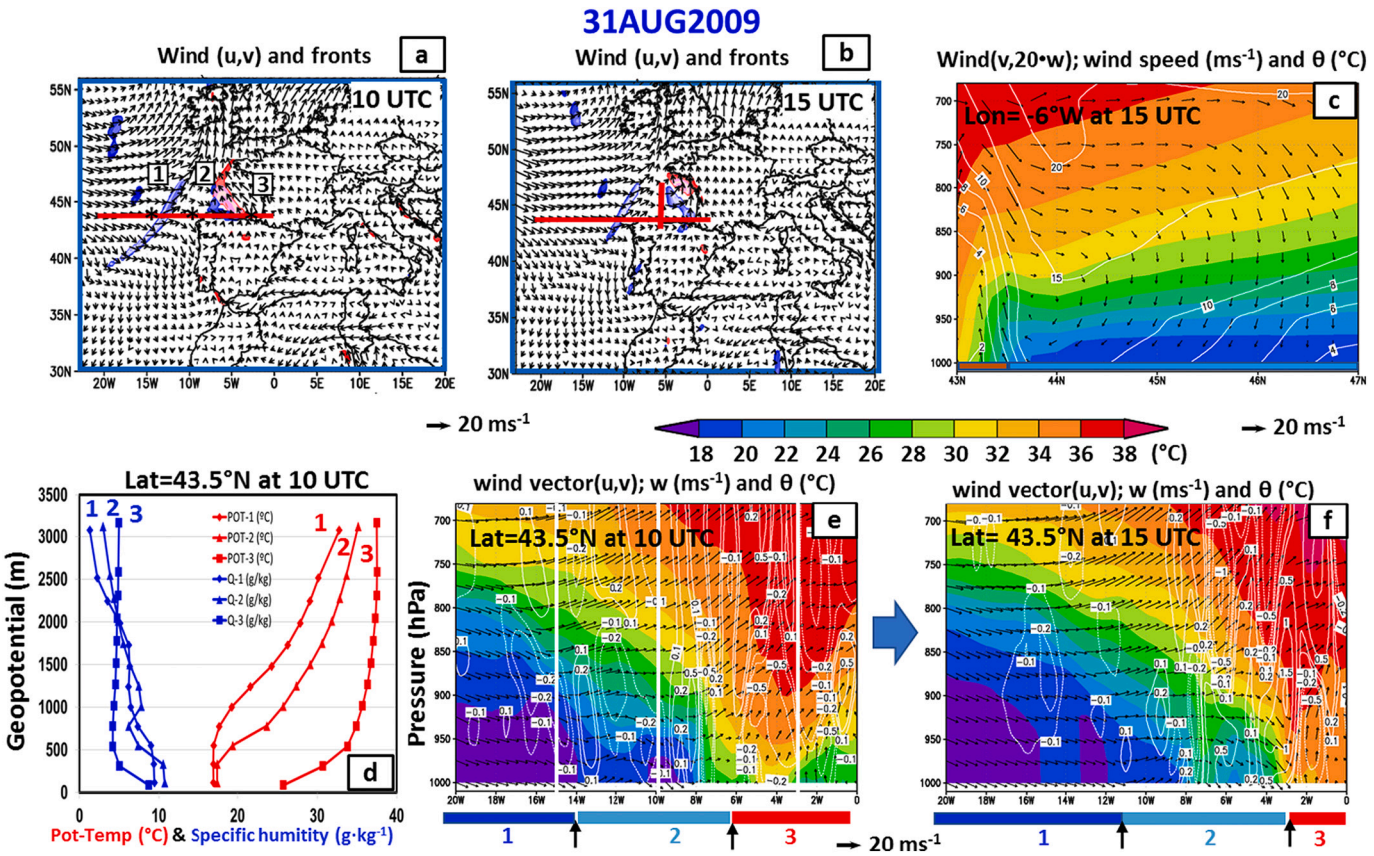

Fig. 5. Vertical cross sections, marked as solid red lines in the (a-b) plant views of Fig. 4 during the propagation of the galerna of 31 August 2009 (a) at 10 UTC, and (b) at 15 UTC, when it is detected in Punta Galea. For the same time instants, the (e-f) constant latitude cross sections of (u, v) wind vectors, (w) vertical winds in contours, and potential temperatures in shaded colors of the three air masses, marked 1-to-3 with arrows and colored bars at the bottom of the (e-f) panels. (d) Potential temperature and humidity profiles at the locations of the solid white verticals in (e), also marked with asterisks in (a). Panel (c) shows a constant longitude (−6° W) cross section of potential temperature in colors, (v, w•20) wind vectors and wind velocities in contours, behind the galerna front. Land-sea surfaces locations are colored at the bottom of the panel. (For interpretation of the references to colour in this figure legend, the reader is referred to the web version of this article.)

positioning of the three air masses at the surface is also represented in colored bars, separated by arrows, which mark the boundaries of the three regions colder (blue)-to-warmer (red). This positioning (14^0 W and 6^0 W, at 10 UTC in Fig. 5e) results from the location of the left boundary of the fronts estimated by our FIS. The pre-frontal shallow cold advection ahead of the parent oceanic front in panels 5e and 5f (air mass 2) is headed by the galerna meso-front, which at 15 UTC is crossing the Punta Galea station (Fig. 5f and Fig. 4d and f). The frontal structure shows similarities with a shallow gravity current with the strong ascent (solid black contour lines in Fig. 4d and f) at the head of the galerna front, in the convergence line between the north-westerlies and the southerlies, and sinking at the rear (dashed red lines in the same figures). The constant longitude cross section in Fig. 5c shows the vertical wind structure at the rear of the galerna front: strong ascent at the windward slope of the coastal mountains and compensatory sinking over the sea. The later contributes to more stabilization on top of the marine cold advection. It is also important to note that the meso-front coastal advance is always facing the air mass 3, a convectively well-mixed boundary layer at the coastal strip. This air mass originates after the Foehn of the continental warm downslope southerly winds at the lee of the coastal mountains (dashed red contours in Fig. 4c and d). This air mass 3, together with the south-easterlies from France, develops a shallow stable MBL farther offshore inside the BB (Fig. 5c), which already occupied the whole BB early in the morning (Gangoiti et al., 2022a), previous to the formation of the galerna front.

The primary oceanic front drawn by the FIS weakens during the advance of the meso-front. It practically disappears on the northwestern coast of Iberia at 21 UTC (Gangoiti et al., 2022a) and it is no longer detected. This behavior is consistent with the more rapid advance of the galerna front with respect to the primary front, the increased convergence into the galerna front, the decreased convergence into the primary front, and the subsequent enlargement of the distance between both fronts (1° longitude, 80 km, in 12 h, from 06 UTC to 18 UTC). Similar process of frontolisis of the primary front and frontogenesis in the pre-frontal through has also been observed in the Type 2 fronts in southern Australia, resulting in an apparent jump in the progression of the primary front (EUMETRAIN, 2012).

3.2. *The case-study of 04 March 2007 (frontal galerna)*

On 4 March 2007, the large-scale weather pattern in Figs. 6a-to-6c has some similarities with the observed in the previous galerna case-study on 31 August 2009. A long-wave trough extends from the North Sea through the west of the British Islands to the west of Iberia, leaving the Azores High far away from the European land mass. This time, the stronger, cold-core, low-pressure system associated with the trough deepens and moves to the North-East, reaching the northern coast of Ireland, while a large amplitude upper-level ridge builds-up to the north over continental Europe. This results in relatively warm southwesterlies blowing over north-western Iberia and the BB at upper levels, which intensify along the day following the increased gradients of the 500 hPa geopotential height, as for the previous case-study. Moderate mean sea level pressure (MSLP) gradients in the BB before 12 UTC (Fig. 6a, b, g, and h) do not match with the strong southwesterlies (10–12 m s^{-1}) observed in the surface stations (Fig. 2c and d), with wind gusts of 19 m s^{-1} at Punta Galea before the frontal passage at 16 UTC. In this case, the

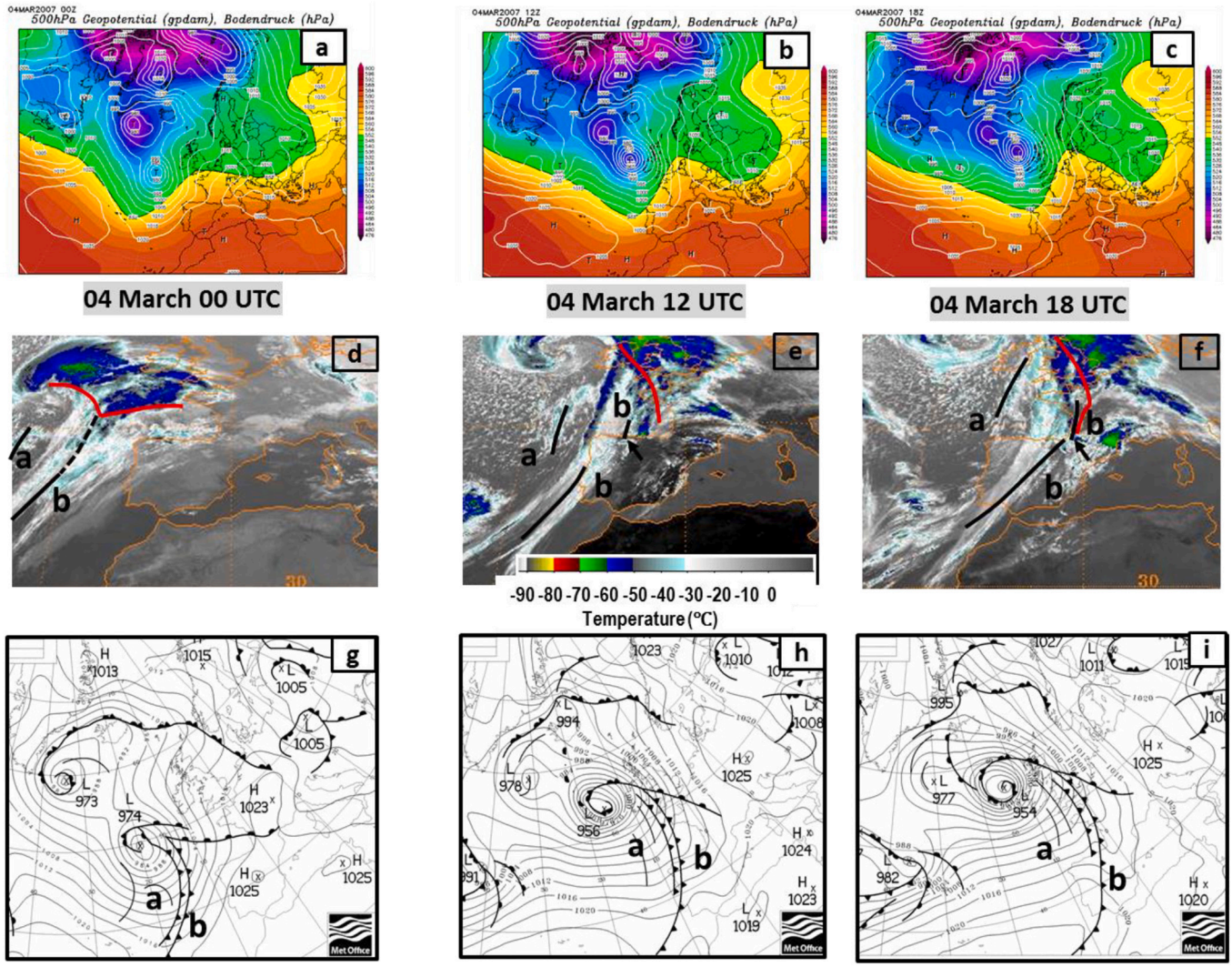

Fig. 6. Synoptic conditions during the galerna of 4 March 2007: as in Fig. 3, same NOAA-NCEP CFSR fields at (a) 00 UTC, (b) 12 UTC and (c) 18 UTC. Simultaneous Meteosat IR (d, e, f) images, and (g, h, i) surface analyses charts. The frontal wind shifts detected by the FIS (Fig. 7) have been drawn on the satellite IR images with both black and red lines in the panels d-to-f. The named a-b front tracks (black and red lines in panels) mark the position of the FIS wind shifts and the arrow the position of the galerna. (For interpretation of the references to colour in this figure legend, the reader is referred to the web version of this article.)

analysis charts of the Met Office (Fig. 6g-to-6i) do show a frontal passage. An Atlantic double front, located at 00 UTC offshore to the west of Iberia, is depicted crossing the BC after 18 h of transit, at the approximate location of the surface stations Punta Galea and Zarautz, before crossing to the southern coast of France (Fig. 6i). A region of anticyclonic vorticity is observed ahead of the secondary front and upstream of the leading trough in Fig. 6h and i. The Meteosat IR image in Fig. 6d shows a region of deep convection over the ocean, to the west and northwest of Iberia at 00UTC (areas of high clouds with blue-green colored cold tops). The black lines a-b in the figure have been drawn at the approximate location of the SW-to-NW wind shift regions detected by the FIS, while the red lines correspond to the *E*-W changes. Lines a and b in the weather chart of the Met Office (Fig. 6g) are approximately concurrent with the location of the trough and the double front, respectively. The dashed black line at 00 UTC in Fig. 6d has been drawn to complete the position of the double front in the IR image, following the directional convergence of the ERA5 south-westerlies, which at this region do not comply with the prescribed FIS wind shifts. Satellite images at 12 and 18 UTC (Fig. 6e and f) document the frontal transit along the Iberian north coast: the front-line b inside the BB at 12 UTC seems to have jumped forward, while in its southern part is lagging behind. Differently from the previous case described in section 3.1, now the galerna front position is marked by a blue colored cloud band, running ahead of line b and marked with an arrow in Fig. 6e and f. At 12 UTC the galerna is around 6^0 W in Fig. 6e. At 16 UTC is crossing Punta Galea (Fig. 2), and at 18 UTC has already crossed the French coast (Fig. 6f), while the double front of the weather charts is still well behind, over the area of Bilbao (Fig. 6i): there is a distance of >100 km between these two points.

The FIS results are shown in Fig. 7. The wind and frontal position are in agreement with the satellite observations in Fig. 6. As for the previous galerna case, described in section 3.1, three air masses can be distinguished in Fig. 7a (00 UTC): the oceanic frontal air mass (number 1) locates behind the westernmost FIS front (in blue), which corresponds to the location of the front line (a) in the satellite image. Relatively cold north-westerlies over a warmer sea develop the observed cloud streets in the satellite image inside this region, with the characteristic parallel bands of cumulus clouds. The double front observed at 00 UTC in Fig. 6 is represented as a unique front by the FIS in Fig. 7a (in blue). As mentioned before for Fig. 6d, the FIS front has been completed with a dashed blue line following the directional convergence of the surface winds, which at this region do not conform with the prescribed FIS wind shifts. Relatively warm south-westerlies blow to the east (air mass 3) with a long trajectory over a cooler ocean, which develops a stable MBL

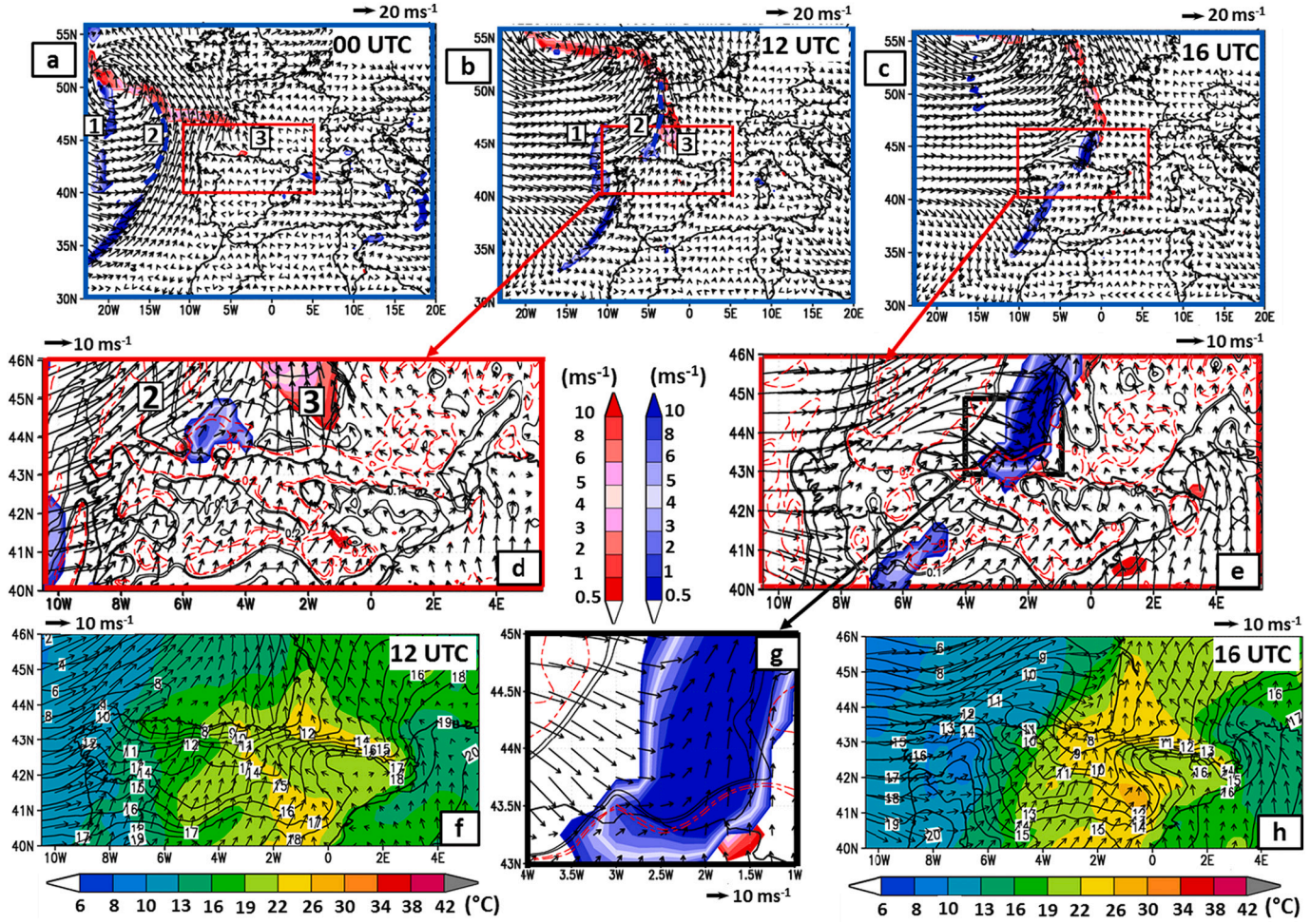

Fig. 7. ERA5 1000 hPa wind vectors and fronts on 4 March 2007: as in Fig. 4, wind shifts before the arrival of the galerna at (a) 00 UTC, (b) 12 UTC, and when it is detected at the Punta Galea surface station (c) at 16 UTC. The enlarged views (d and e), show wind vectors, wind shifts and vertical wind speeds, and panels (f) and (h) potential temperatures and mean sea level pressures. Panel (g) shows a detailed plant view of the galerna mesofront while crossing Punta Galea.

and forms the red-colored FIS region in the northern boundary of the BB in Fig. 7a. This is the location of the warm front associated to the Atlantic depression in the weather charts (Fig. 6g) and, following the IR satellite image (Fig. 6d), the region shows deep blue-colored clouds to the north of the red line, which mark the approximate position of the warm front. The same air-mass (3) is observed at 12 UTC crossing the north-west corner of the Iberian Peninsula to the north coast and sinking into the BB, which causes both the downslope winds at the lee of the coastal mountains and a new MBL, which grows from south to north inside the BB (Fig. 8b). The air mass (2) locates between the two blue colored fronts, marked as lines (a) and (b) on the satellite images, and it is running behind the double front. The wind in this region is from the south-west near the leading front (b) and more from the West at the rear, close to the front-line (a). As it will be shown next, its thermal characteristics are intermediate between the air masses 3 and 1. This air mass (2) will develop the galerna, which will cross the target area in the afternoon. Following the ERA5 surface wind shifts, temperature, and pressure data, the galerna initiates between 11 and 12 UTC, close to the point of Cape Peñas at around 6^0 W (Fig. 7d and f), marked in blue in the boundary between air mass 2 and 3, at the moment when the colder MBL faces the low-pressure area to the East (Gangoiti et al., 2022a). As for the previous case-study, there is a mesoscale ridging in the oceanic air mass (2) to the west of the coast, concurrent with the cold air advection and a simultaneous troughing of the continental southerlies at the coastal strip during the development and intensification of the galerna front (Fig. 7f and h). Winds behind the front do not reach the geostrophic balance during their propagation thought the BB. As for the previous case study, lee troughing could have both a thermal and a dynamic origin, because both components can act simultaneously after the intense Foehn in the coastal area preceding the galerna front.

The trapped surface winds in the MBL turn anti-cyclonically in Fig. 7e in response to the local pressure gradients developed between the marine cold advection and the warm continentals blowing ahead (Fig. 7h). This anticyclonic turning of the south-westerlies of the air mass (2) into the coastal leading trough increases the convergence downstream and sharpens the galerna front. Winds behind the galerna front are far from reaching the geostrophic balance and cross the isobars directly into the low pressure. Simultaneously, a large area of sinking over the marine advection (2) is observed behind the galerna front in Fig. 7e (dashed contour lines). This is consistent with the observed cloud dissipation between lines (a) and (b) in the IR images during the front propagation in the northern coast, and the divergence behind the front, with a weakening of the trailing FIS front-line (a) as observed in Gangoiti et al. (2022a).

ERA5 wind and potential temperature vertical cross sections are shown in Fig. 8. As for the previous case-study, the three air masses (1-to-3) involved in the development of the galerna front are represented in Fig. 8a. The corresponding three vertical profiles of ERA5 potential temperature and specific humidity are represented in Fig. 8d. They locate at the same latitude (43.5 °C) and at longitudes 14^0 W, 11^0 W, and 3^0 W (Fig. 8e). As for the case of the non-frontal galerna in section 3.1, the surface temperature values in the verticals (1) and (2) are equal, and

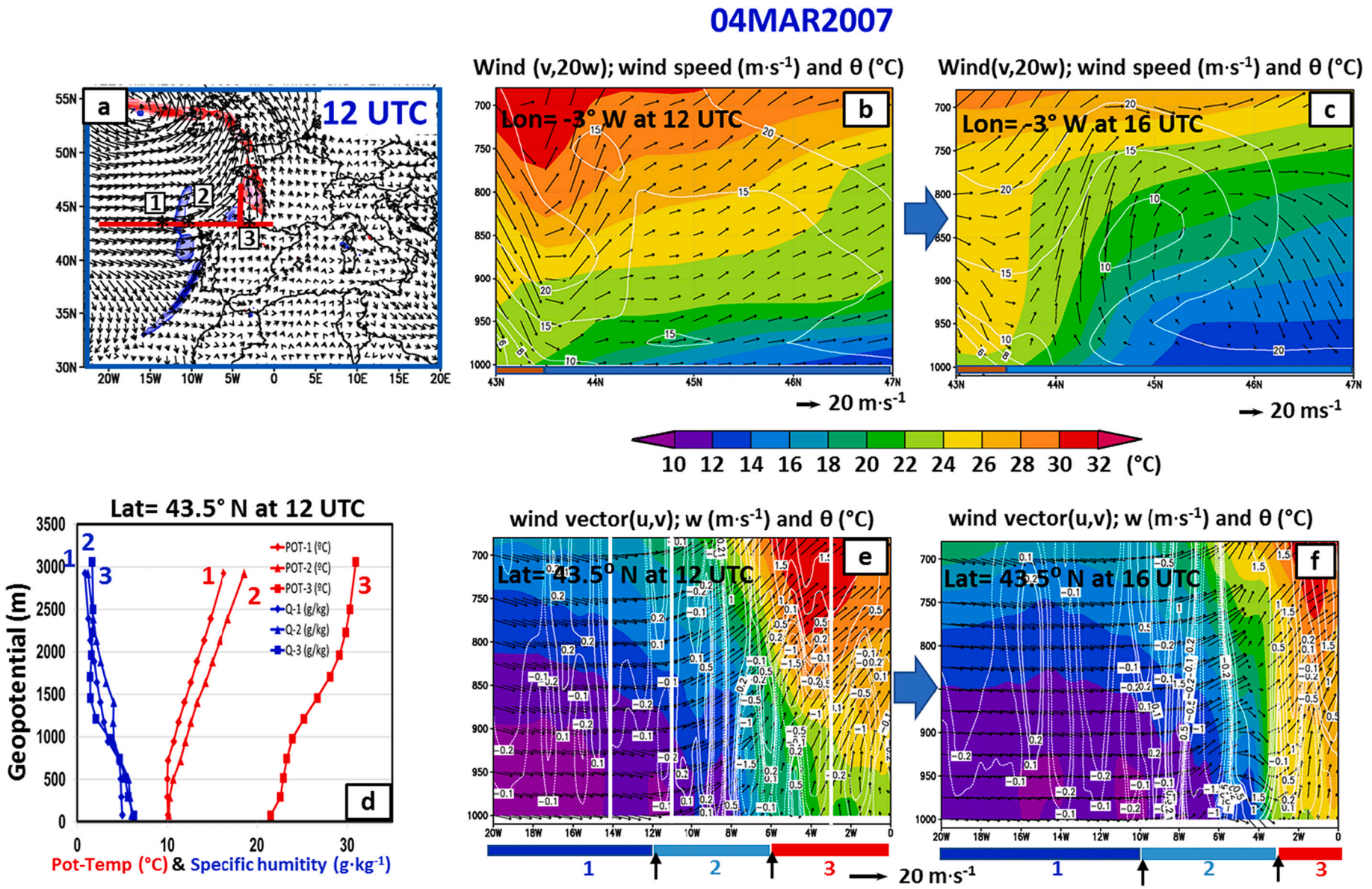

Fig. 8. Vertical cross sections, marked as solid red lines in the (a) plant view of the Fig. 7 during the propagation of the galerna of 4 March 2007, (b, e) at 12 UTC and (c, f) at 16 UTC when it is detected in Punta Galea. As in Fig. 5, the constant latitude cross sections (e, f) show the temperature and wind fields throughout the three air masses (marked 1-to-3) with arrows and colored bars at the bottom of the (e-f) panels. The simultaneous constant longitude cross sections (b) and (c) at 3° W, show the same fields as in Fig. 5. Panel (d) shows potential temperature and humidity profiles at the locations of the solid white verticals in (e), also marked with asterisks in (a). (For interpretation of the references to colour in this figure legend, the reader is referred to the web version of this article.)

they seem to be conditioned by the temperature of the sea surface. They show a well-mixed MBL (almost constant potential temperature and specific humidity) with a relatively cool and moist air mass capped by the drier south-westerlies of the free atmosphere, which at this time locates above an altitude of 800–1000 m ASL. Point 3 is located offshore, and the vertical temperatures are much higher (>10 °C) than the temperature of the air masses (1) and (2). It shows a well-mixed MBL of around 1000 m height, with a developing (200 m height) stably stratified internal boundary layer which grows northward (Fig. 8b) within the continental southerlies preceding the galerna front. The land and sea locations are represented at the bottom of this figure in red and blue colored closed rectangles, respectively. While this cross-section (Fig. 8b) represents the air mass (3) close to Punta Galea (lat = 43.37^0 N, lon = 3.03^0 W) before the frontal crossing, Fig. 8c represents the same cross-section at the time of the frontal passage. Here, the downslope Foehn is still observed inland, while the wind ascent offshore is marking the position of the galerna-front on the sea, consistent with the FIS results (Fig. 7g). A similar sequence of wind and temperature cross-sections, before and at the time of the galerna occurrence at Punta Galea, are shown in the constant-latitude cross-section of Fig. 8e and f. As in Fig. 5, they show the progress of the three air masses between 12 UTC and 16 UTC with their respective positioning at the bottom, represented in colored closed rectangles, separated by arrows, which mark the boundaries of the three regions. There are important similarities with the galerna represented in Fig. 5: the increasing horizontal temperature gradients during its development, the strong ascent at its leading edge when crossing the Punta Galea point (between 5^0 W and 3^0 W), and the sinking at the rear over the colder marine advection.

4. List of galerna events (2003–2020) and climatology: Sensitivity analysis, validation and classification

After the application of the EIS (section 2.2) to the identification of galernas during the 18-year period 2003–2020, the results are summarized in Fig. 9a. We have identified a total of 85 galernas during the referred period. The dates are distributed by months and years and, on average, there are about four-five episodes per year, with a large inter-annual variability (Fig. 9b), where the minimum was in 2013, with just one episode, and maxima of seven cases occurred in 2003 and 2009. The months of May and June concentrate the largest fraction of episodes: an average of almost one episode per year in each of these two months (Fig. 9c). After June, their monthly frequency decreases to reach a minimum of zero episodes in December and January, and increases during the spring season (March–April) up to 0.5 episode/month.

Four galernas have registered wind gusts over 30 m s^{-1} (108 km h^{-1}) at Punta Galea, with the strongest one (139.7 km h^{-1}) on 15 July 2007. Zarautz registers weaker winds, probably because of the coastline local curvature and height, and its maximum was registered on 28 April 2003

a

LIST OF GALERNAS (18 YEARS)

	JAN	FEB	MAR	APR	MAY	JUN	JUL	AUG	SEP	OCT	NOV	DEC	YEAR TOT
2003			05	28, 29	02, 19	13		27					7
2004						22		11, 19					3
2005				06	25, 27	27				12, 28			6
2006				15	17	08, 10	01, 27						6
2007			04	24		19	15						4
2008			15	29	07, 23		23						5
2009							22	01, 23, 31		05	01, 14		7
2010			29		09					29			3
2011			26			27		6, 20					4
2012			17		10, 25	21, 27		27					6
2013				14									1
2014		20		23		06, 28					13		5
2015					07	04	3, 10	02		27			6
2016		26	30					25	07, 13				5
2017			03		05, 25				14	16, 21			6
2018									17	11			2
2019				15	08	18, 26, 27			21				6
2020					04	11					02		3
MONTH TOT	0	2	8	9	15	16	7	11	5	8	4	0	85

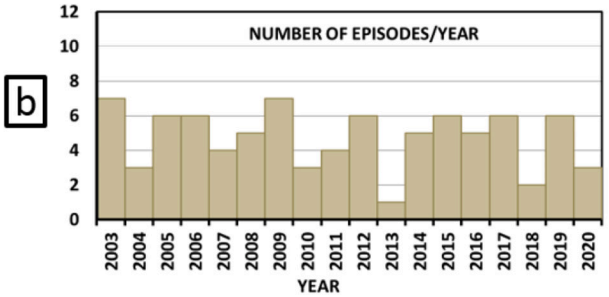

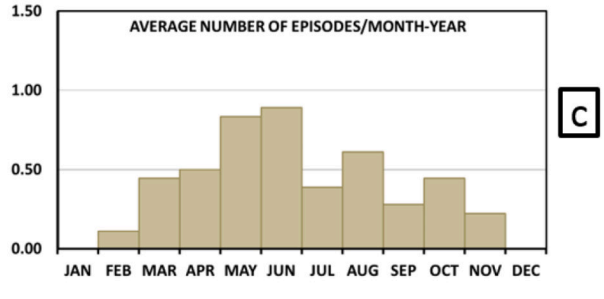

Fig. 9. (a) List of all the (85) galerna events identified by the EIS during the 18-years (2003–2020) period. The number of events distributed by (b) years and (c) months show a large inter-annual variability and a clear preference for the months of May and June, with an average (interannual) frequency of almost one episode per year in these months.

(103 km h^{-1}), while Punta Galea registered 110 km h^{-1} during that episode. Using the reaching time of all the galerna-events to the station of Zarautz, they show a frequency distribution (Fig. 10a) with maximum between midday (12 UTC) and late afternoon (21 UTC). The stronger galernas are also registered during this time lapse, as shown in the box plots (Fig. 10b and c) of the hourly distribution of wind maximums of the 85 galernas detected in both surface stations.

The list of the 85 galerna events (Fig. 9) holds for the set of the prescribed parameters (reference selection in section 2.2), which are based on the mentioned two surface station's wind and temperature data and the ERA5 reanalysis. If we change the parameters the list changes. A more restrictive condition of $Fr_m < 0.7$ (prescription number 6 in section 2.2) leads to a reduction of the number of galernas from 85 to 69. Alternatively, the removal of the condition related to the Fr_m leads to an increase of identification from 85 to 102 galernas, as observed in Fig. 11 a1 and b1: all new cases add to the cold months, September to December and January to March. We interpret these results as a consequence of having more unstable conditions of the marine advections during the cold months, with relatively cold airmasses over a warmer sea, which prevents the coastal trapping and the wind channeling effects needed for the development of galernas.

Changing the rate of the temperature decrease ($-\Delta T/1\ h > 4\ °C$) has also a direct effect in the resulting list of identifications. In Fig. 11 a2 and b2, we show the effect of doubling the rate to $-\Delta T/0.5\ h > 4\ °C$. The result is a reduction of the positive identification cases to 63 galernas with respect to the reference selection (85). Attending to the monthly frequency distribution (Fig. 11 b2), and comparing with the reference selection, we can conclude that even though there is an increase in the number of cases with an abrupt temperature drop in May and June it is not as severe as the reduction of cases in the other months, although there still are cases in every month from February to November.

The EIS is also sensitive to changes in the wind intensity. In Fig. 11 a3 and b3 it can be seen the effect of increasing the wind gust maximum (V_{max}) from 50 km h^{-1} to 72 km h^{-1} (20 m s^{-1}). There is an important reduction of the cases to 45, distributed along all the (18) years, included 2013, which only showed one case in the reference selection. Consequently, despite the reduction in their number, strong galernas can happen in practically every month of the year. In addition, the monthly frequency distribution does not show such a large difference between May–June and the rest of the months, denoting a reduced seasonality. Thus, we can conclude that (1) at least one strong galerna can happen in any year and (2) the strongest galernas can happen at any month of the year between February and November and with a similar probability.

The sensitivity analysis has allowed us to obtain valuable information of the characteristics of the galernas. However, an important caveat about the results of the EIS is that the final list is dependent on the selection of surface stations, parameters, and the prescribed limits. Consequently, the comparison/verification by using other previous (shorter) list of galernas has been challenging because they have been usually made by using other surfaces stations, other parameters and limits, and, unexpectedly as far as we know, no stability criteria (Froude and wind shear). Nonetheless, there is a general agreement with the available lists of the galerna events identified for the same period. Eleven cases (79%) of the list of the fourteen galernas identified in the period 2003–2011 in Gaztelumendi et al. (2011) are included in the reference list in Fig. 9a. For the remaining three cases (18 June 2005, 14 February 2007 and 30 April 2007), either the vertical wind shear, the Froude number, or an insufficient hourly rate of the temperature decreases are out of our reference prescriptions. Liria and Aranda (2013) add seven new cases for the same period 2003–2011, and four are out of the prescriptions for similar reasons: in this case, Froude, wind shear and a relative low wind maximum. More recently, during the last decade, an increased number of videos of galernas can be found on the web, more likely related with an increased use of smart phones and other portable devices for digital video recording. In the Appendix of this article, we have include a Table with a list of galernas, which can be found in YouTube (since 2012). The link and date of each event is included as well as a comment on its eventual inclusion in the reference list in

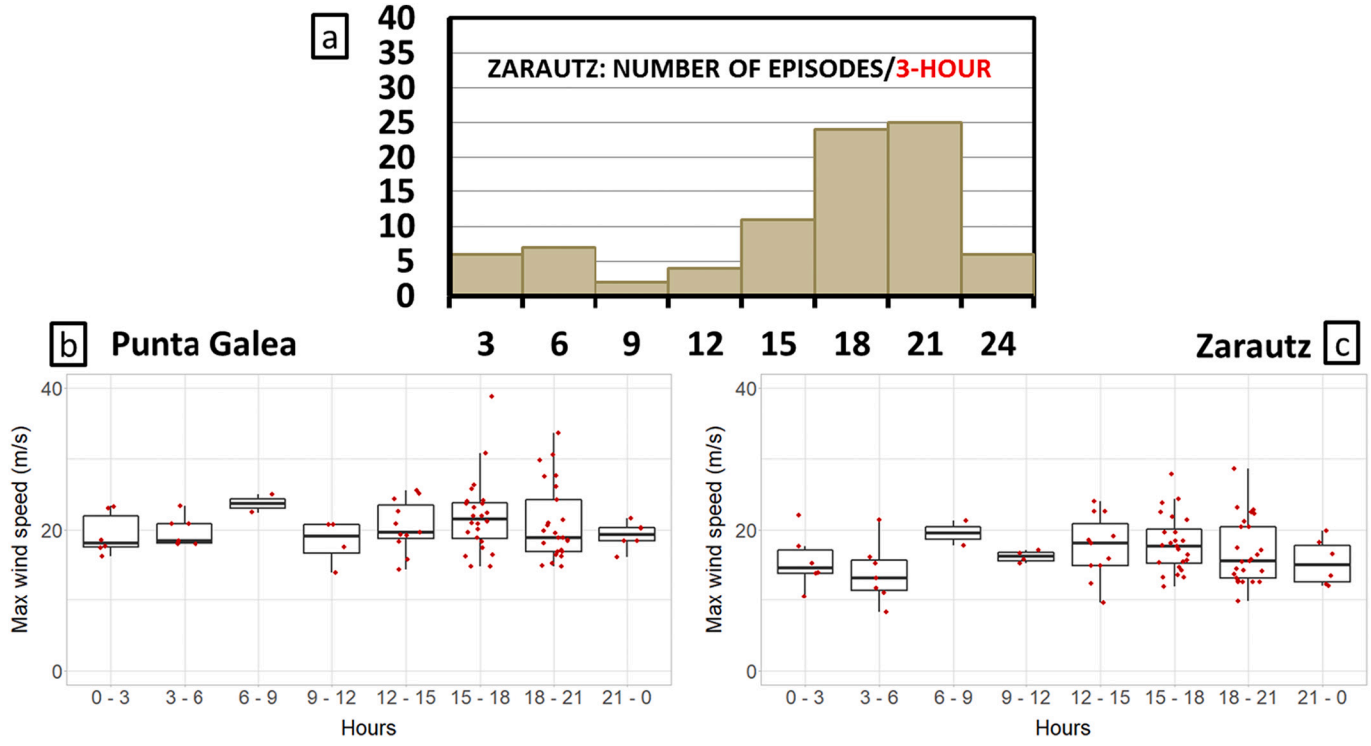

Fig. 10. (a) The frequency distribution of the detection time of the (85) galernas in the reference list at the Zarautz surface station shows maximum values between midday (12 UTC) and late afternoon (21 UTC). The box plots of the hourly distribution of wind maximums in (b) Punta Galea and (c) Zarautz show that the strongest galernas are also registered during this time lapse.

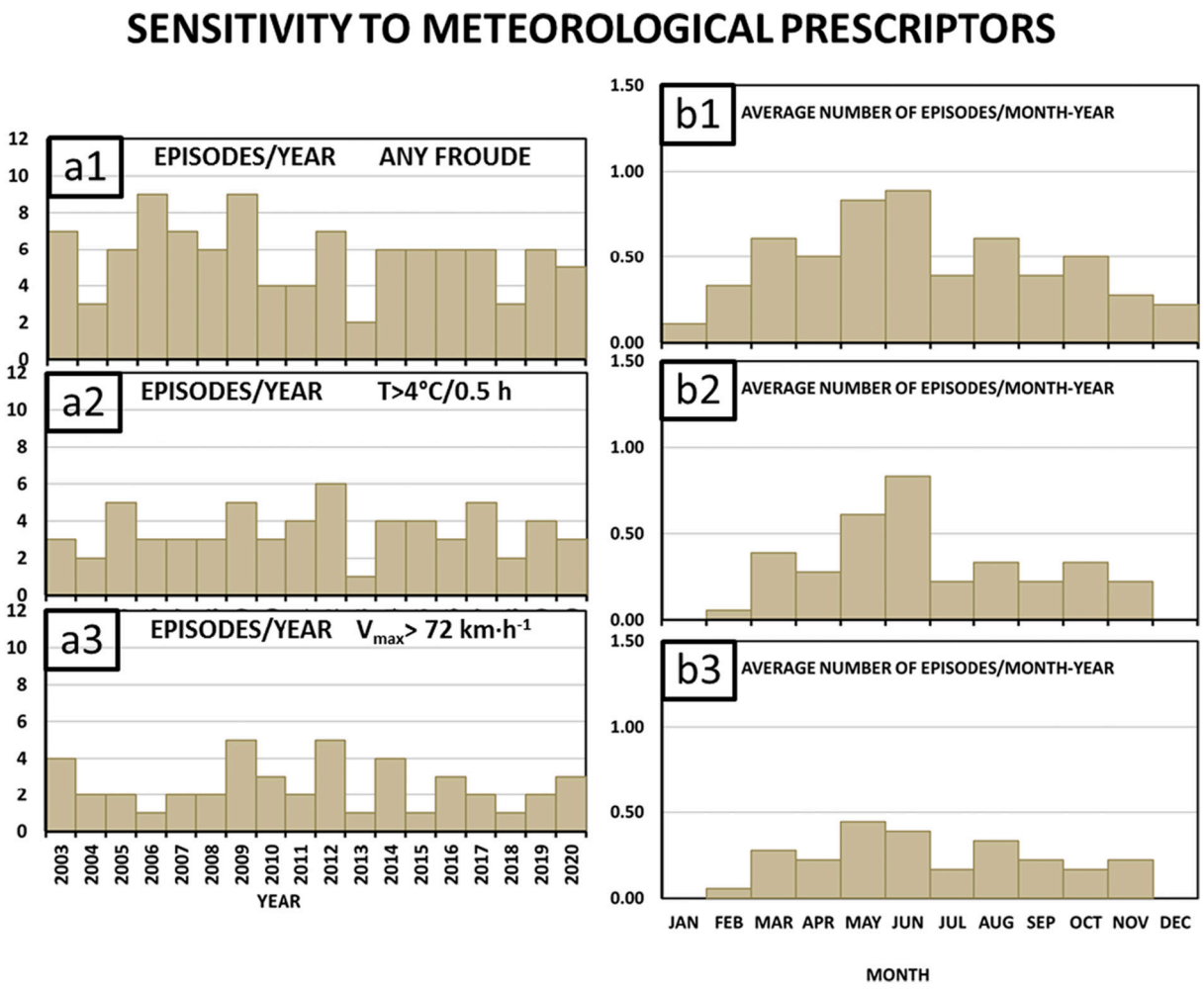

Fig. 11. Sensitivity of the EIS to changes in the meteorological prescriptors. The removal of the condition related to the mountain Froude number, (a1) increases the number of events in most of the years and (b1) the monthly distribution changes respect to the reference list in Fig. 9. Doubling the rate of the temperature decreases ($-\Delta T_{crit}$) has a direct effect in both (a2) the resulting (decreased) list of identifications and (b2) the enhanced seasonality in its monthly distribution. Increasing the wind gust maximum ($V_{máx}$) from 50 km·h^{-1} to 72 km·h^{-1} decreases the seasonality and the number of galernas.

Fig. 9a. Seven cases (70%) are on the list, while for the remaining three cases, the Froude number and a relative low wind maximum are out of prescriptions.

The new ERA5 hourly reanalysis has allowed us to introduce the vertical stability criteria for the identification of galernas after its improved time-space resolution and reliability. The later due to an increased number of assimilated observations, including new satellite products and reprocessed climate data records among other advances with respect to the former 6-hourly ERA-Interim reanalysis (Hersbach et al., 2020; Bell et al., 2020). Despite this, in a reduced number of cases, we have found inconsistencies between the wind field representation of the ERA5 and the observations at the selected coastal stations. This is the case of the galerna of 13 June 2003. Exceptionally, at that time, two successive galernas occurred in <24 h (13–14 June 2003): only the first one, on June 13, complied with the wind/temperature prescriptions in the surface stations. The second one was not strong enough and kept below the V_{max} requirements. However, the first one was captured by the EIS although the simultaneous ERA5 surface wind velocity values (4 m s^{-1}), not used by the EIS, were well below the observations (15–16 m s^{-1}).

Galerna events are classified as frontal and "non-frontal", depending on whether they are caused by a synoptic Atlantic front or by a local micro-front originated in the coastal area of northern Spain, respectively. If we consider the total list of 85 galernas of the EIS reference selection in Fig. 9a, only 14 (16.5%) were frontal galernas caused by synoptic-scale fronts originated out of the BB, while the remaining 71 (83.5%) have a local origin, which would correspond with the "non-frontal" galernas with a relative short life of several hours. All of them are coastally trapped disturbances or wind reversals, and the FIS have tracked their position (hourly) during their whole life span on the northern coast of Spain. The sequence of the front formation in both the large (g1) and the small (g2) domains for all the 85 cases of the EIS reference list, including the galerna of 25 July 1995, can be download from the ZENODO repository (Gangoiti et al., 2022a)

5. Averages, anomalies, and main synoptic patterns

Fig. 12 (middle column) represents the surface and middle troposphere averages of a selection of ERA5 meteorological variables during the 85 galerna events of the reference list in section 4 at the time of the detection of each galerna front at Zarautz. The inter-annual averages (climatology) are represented in the left column of the figure, and the anomalies (the differences between the composite "average galerna" and the inter-annual averages) in the right. Fig. 12a and b represent the 1000 hPa (m) and 500 hPa (dam) geopotential heights in contour lines and shaded colors, respectively, while the anomalies of these fields (m) during an "average" composite-galerna (Fig. 12b) and the climatology (Fig. 12a) are shown in Fig. 12c. The high-pressure (positive) anomaly at

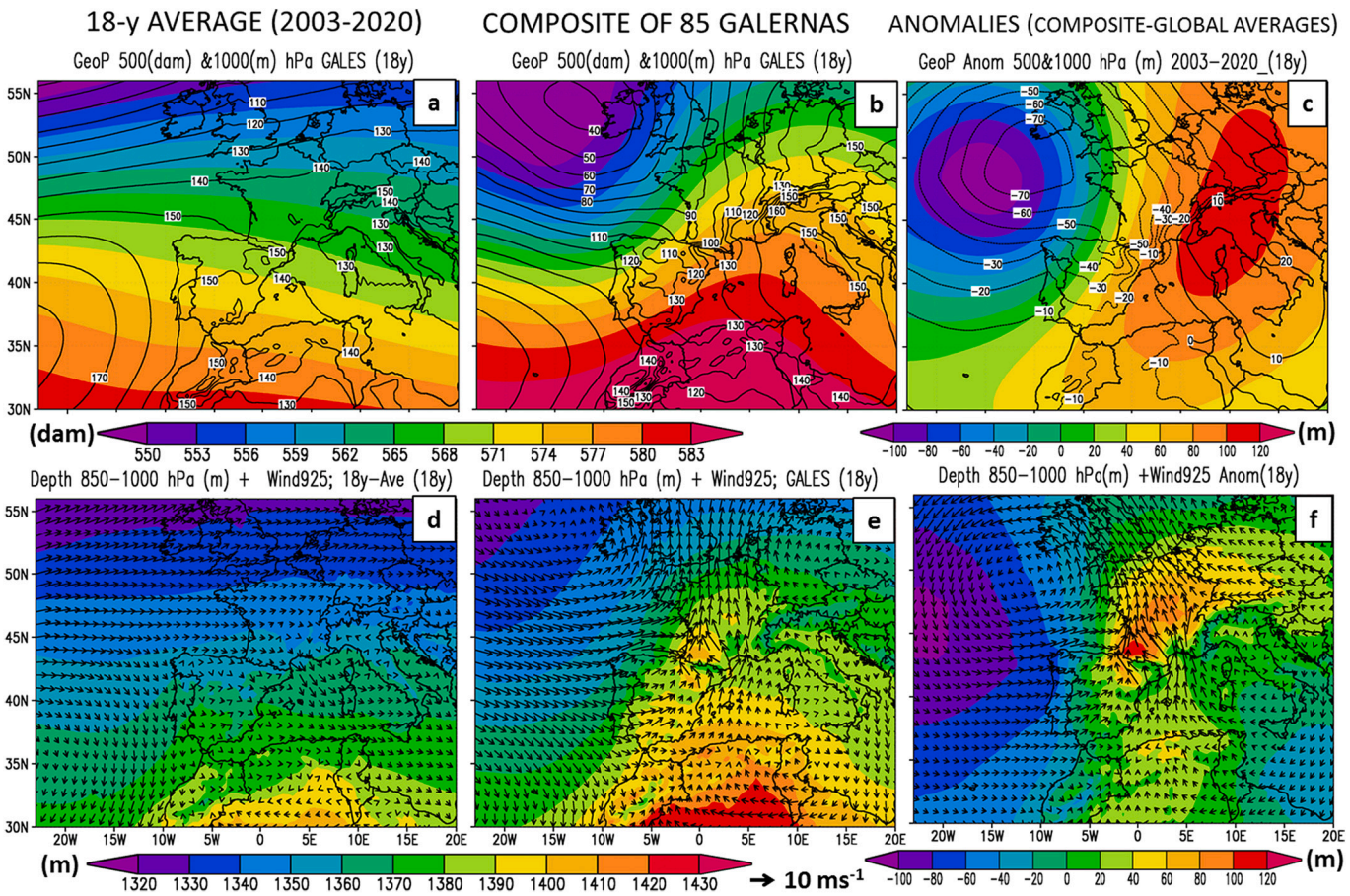

Fig. 12. ERA5 18-y average (2003–2020) of the (a) 500 hPa (dam) and 1000 hPa (m) geopotential heights in shaded colors and contours, respectively and (d) the 850–1000 hPa thickness (m) and 925 hPa wind vectors for the same period. Two composite (b, e) of the same meteorological variables are shown for the reference list of galernas, at the time of their detection in Zarautz. The anomalies (c) and (f) are the difference between the composite and the inter-annual averages in the middle and left columns, respectively.

upper levels over continental Europe (Fig. 12c) corresponds to the higher frequency and intensity of upper-level ridges from northern Africa to northern Europe during the documented galerna events. This represents an important blocking pattern over continental Europe, which prevents the normal eastward motion of depressions in the zonal flow. Alternatively, the Atlantic region to the northwest of the BB shows a low-pressure (negative anomaly) at upper levels. The average synoptic pattern (Fig. 12b) forces warm south-westerlies at upper levels and cold advections from the west at the surface on the northern coast of Iberia, which is a recognizable pattern of these events. This is true at the time of the galerna frontal passage at Zarautz. Consequently, the figures do not show the prevailing surface warm continental offshore winds into the BB, which precede the galerna meso-front formation, as described in section 3.

The 850–1000 hPa thickness (m) and the 925 hPa wind vectors are represented in Figs. 12d-to-12 f. The thickness defines the mean temperature of the lowest 1500 m or so, and the wind vectors represent the prevailing winds in that layer, which includes the MBL in the northern coast. A warm anomaly is observed at the eastern corner of the N-Iberian coast, the Ebro valley, and at the lee of the Basque Mountains and Pyrenees in southern France (Fig. 12f), and a cold one to the west, on the Atlantic Ocean. This is consistent with a heated air mass over a warmer landmass (thermal low) transported to the North within the southerlies. This air mass locates ahead of the galerna front at the coast and contributes to sharpen the coastal pressure gradient relative to the marine cold advection from the west.

The mean synoptic pattern associated with the galerna events, represented in the composite of the Fig. 12 (middle column), hides a variety of atmospheric processes and synoptic patterns leading to their development. Thus, the galerna event of 2 November 2020 (Fig. 13 a1) does show a similar pattern to the observed average (Fig. 12b). It has a long Rossby wave around the same region in northeastern Atlantic, a blocking ridge of high pressures to the East in continental Europe, and a surface pressure field compatible with a cold advection into the BB. The events of 17 September 2018 and 04 March 2007 (Fig. 13 a2 and a3) have also similarities with the average pattern in Fig. 12b. The former (Fig. 13 a2) shows the time instant of the merging of the ex-tropical storm Helene into the main stream, to the NW of Iberia. The subsequent surface pressure changes induced in the BB could have had a role in the triggering of the observed galerna event of that day (17 September 2018).

A similar blocking ridge of high pressures is also observed in the rest of the galerna events shown in Fig. 13. However, the pressure pattern in the Atlantic shows a variety of cases. In panels 13b1-to-13b3 an upper-level low locates to the West of Ireland, which for the case of 02 August 2015 is in association with a deep mid-latitude cyclon at the surface. In all cases a surface low-pressure region develops to the southeast of the upper level low inside the BB, which drives the cold westerly advection in the coastal region, responsible of the onset of corresponding galernas. A different Atlantic pattern is shown in the three panels 13c1-to-13c3, with the synoptic conditions before the onset of the subsequent three galernas in panels 13d1-to-13d3. This time an upper level low (or trough) locates to the west of Portugal, and a shallow surface depression heading these lows moves to the BB anticipating the galerna events of panels 13d1-to-13d3.

Eight of the nine galerna events illustrated in Fig. 13 correspond to

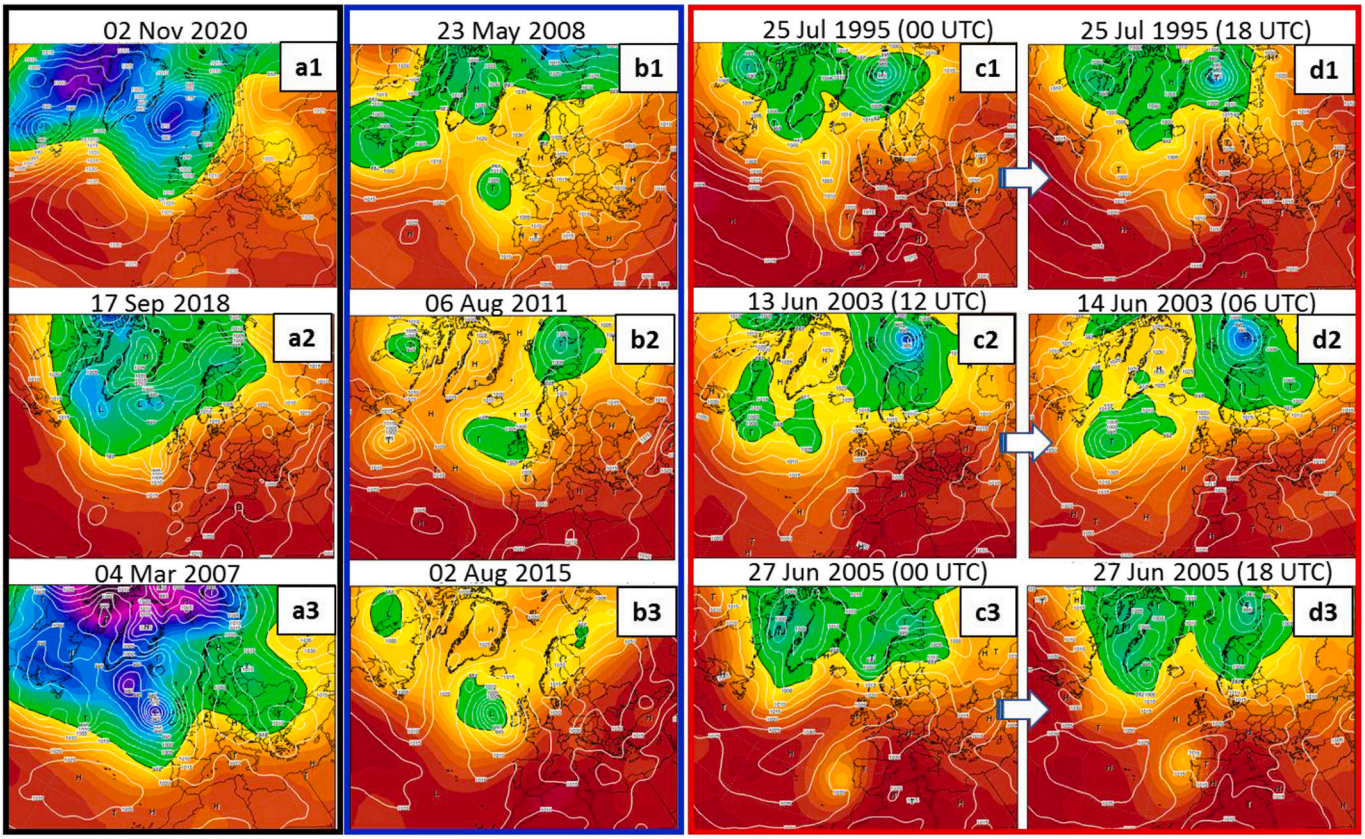

Fig. 13. Synoptic patterns of the galerna events (three types). (1) Large upper-level troughs (a1 to a3), which extend N-to-S from Island to the west of Iberia. (2) Upper-level lows (b1-b3) located to the west of Ireland, sometime in association with a deep mid-latitude cyclon at the surface (02 August 2015). (3) Upper level lows (or troughs) located to the west of Portugal (c1 to c3): shallow surface depressions heading these lows can move to the Bay of Biscay and develop (d1 to d3) the galerna events. The upper-level ridge, which extends from northern Africa to western France is a common pattern in all the panels.

cases detected by the EIS (section 4). Exceptionally, the case represented in panels 13c1 and 13d1 is the well-documented "historic" galerna of 25 July 1995 (Arasti, 1999, 2001) which occurred before the initial date selected for the present study. Two of them (in Fig. 13) were fronts initiated in the Atlantic Ocean, out of the BB: 02 November 2020 and 04 March 2007. The later has been described in section 3.2. The remaining cases correspond to local frontogenesis ("non-frontal" galernas).

6. Summary and conclusions

We have designed an objective methodology for the identification of galernas, using specific temperature, wind, and stability criteria, named EIS. Its application produced a list of (coastally trapped) galerna events in the BB, leaving other features, as their seasonality and preferred afternoon-evening time of occurrence, to be a consequence and not a pre-requisite of the designed EIS. Both surface stations wind and temperature data and the ERA5 hourly reanalysis have been used in its design. Using the prescriptions of the EIS reference study, we have identified 85 galernas during the period 2003–2020. A frontal identification system (FIS) has also been designed, based exclusively in the ERA5 hourly reanalysis. The FIS has been a great help to observe the development of the galerna events previously identified by the EIS: most of them (83.5%) have a local origin inside the Bay of Biscay and the remaining (16.5%) are oceanic fronts initiated out of the region. The local frontogenesis is more frequently initiated by the relatively cold marine southwesterly pre-frontals preceding a parent oceanic front and blowing against the warm continentals, which spread over the BB. This local frontogenesis preceding the parent front seems to be the reason of the apparent jump of the primary front, which eventually can weaken and even disappear. Even in the case of the more occasional frontal galernas directly caused by the westerlies or north-westerlies behind an oceanic front, their eastward propagation is more rapid over the maritime BB region. Thus, the front deforms in shape (01 November 2009, 17 March 2012, 02 November 2020 in Gangoiti et al., 2022a), and may cause its unexpected and abrupt irruption in the target area.

The EIS reference selection of galerna events during the period 2003–2020 has shown that all of them occur under a synoptic high-pressure (positive) anomaly at upper levels over continental Europe. These conditions correspond, most frequently, to synoptic scale upper-level ridges, which extend from northern Africa to northern Europe. This characterizes a blocking pattern over the continent, which prevents the normal eastward propagation of depressions in the zonal flow. Conversely, the pressure pattern in the Atlantic shows a variety of cases. The observed average synoptic conditions force warm south-westerlies at upper levels over the BB region, with Foehn and warm continental offshore winds at the surface on the northern Iberian coast, which can also blow from the east-southeast at the French Atlantic coast. Simultaneously, surface cold advections are forced from the west over the target region, most frequently associated with a low-pressure system and/or oceanic front, which could initiate the referred local frontogenesis, enhanced by the simultaneous lee troughing of the continental southerlies at the coastal strip during the development and intensification of the galerna front. The lee troughing could have both a thermal and a dynamic origin, acting simultaneously after the intense Foehn in the coastal area preceding the galerna front. The signature of the thermal low in the easternmost region of the BB can be observed in the 850–1000 hPa average thickness (m) and the anomalies of the climatology of the detected galerna events. The thermal lows show the greatest intensity during the afternoon, which could be an important argument to explain both the preferred timing of the galernas at crossing

the target area and the time-lapse occurrence (12–21 UTC) of the most intense events.

The target area receives an average of four-to-five galernas a year, with a large inter-annual variability: one-to-seven events per year, with no apparent trend in the 18-year record. May and June concentrate the largest fraction of episodes, with an average of almost one episode every May and June in every year. Their number decrease during the summer and fall season to reach a minimum of zero events during December and January, and increases rapidly during the spring season (March–April) with an average of up to 0.5 episode/month. They occur more frequently between midday and late afternoon and the strongest ones concentrates during this daytime period. Four galernas have registered wind gusts over 30 m s^{-1} (108 km h^{-1}) at Punta Galea, with the strongest one on 15 July 2007 (14 UTC), originated by local frontogenesis: the parent oceanic front, though, never crossed the target region (weather charts and FIS results in Gangoiti et al., 2022a). Strong galernas ($V_{max} > 72$ km h^{-1}) have occurred in all the (18) years of this study. They can happen in any month, from February to November, with a similar probability. On the contrary, the highest rates of temperature decreases ($-\Delta T/0.5\ h > 4$) do have a more marked seasonality: May and June show a somewhat larger number of cases with an abrupt temperature drop with respect to the other months, although there still are abrupt drop cases in every month from February to November. The higher temperature contrast during the spring season between the marine and continental airmasses, facing each other during a galerna event, could be behind these results. Our sensitivity analysis of the EIS has shown that fronts detected at the surface stations, without the Fr_m prescription, add a few more new cases to the cold season with respect to the warm season of each year (from September to December and January to March). This could be related with the more unstable conditions of the autumn-winter marine advections, which prevents the coastal trapping and mountain channeling of the wind and favors a vertical loss of energy in a non-trapped marine boundary layer.

The national and regional meteorological services in Spain and France activate galerna warnings whenever there is a risk of their formation after the results of their numerical modelling. In spite of the important progress of the weather services capacities, forecasting their initiation, intensity, and arrival time is still quite challenging. The described ingredients and the assessed list of the more recent historical galernas could help not only to improve our understanding of this phenomenon but also to their more accurate forecasting.

Data availability statement

All the meteorological data of the surface stations used in this article are available through

https://euskalmet.beta.euskadi.eus/s07-5853x/es/meteorologia/datos/mapaesta.apl?e=5

The hourly ERA5 reanalysis on pressure levels can be download from the Climate Data Store (CDS) of the Copernicus Climate Change Service (C3S) https://cds.climate.copernicus.eu/cdsapp#!/dataset/reanalysis-era5-pressure-levels?tab=overview The satellite images included in the article can be download from https://www.ncdc.noaa.gov/gibbs/year The site belongs to the International Satellite Cloud Climatology Project (ISCCP) at the NOOA's Global International B1 Browse System (GIBBS).The 6-hourly surface analyses charts produced by the UK Met Office were download from https://www2.wetter3.de/) and the satellite images from the NOOA's Global International

CRediT authorship contribution statement

Gotzon Gangoiti: Conceptualization, Data curation, Formal analysis, Funding acquisition, Investigation, Methodology, Validation, Visualization, Software, Writing – original draft, Writing – review & editing. **Ana Rodríguez-García:** Conceptualization, Data curation, Software, Visualization, Writing – original draft, Writing – review & editing. **Estibaliz Sáez de Cámara:** Conceptualization, Methodology, Supervision, Writing – original draft, Writing – review & editing. **Eduardo Torre-Pascual:** Conceptualization, Data curation, Software, Visualization, Writing – original draft, Writing – review & editing. **María Carmen Gómez:** Conceptualization, Methodology, Supervision, Writing – original draft, Writing – review & editing. **Maite de Blas:** Conceptualization, Data curation, Methodology, Visualization, Writing – original draft, Writing – review & editing. **José Antonio García:** Conceptualization, Funding acquisition, Methodology, Writing – original draft, Writing – review & editing. **Estíbaliz García-Ruiz:** Conceptualization, Methodology, Supervision, Writing – original draft, Writing – review & editing. **Iñaki Zuazo:** Conceptualization, Methodology, Writing – original draft, Writing – review & editing. **Verónica Valdenebro:** Conceptualization, Methodology, Writing – original draft, Writing – review & editing. **Jon Iza:** Conceptualization, Methodology, Writing – original draft, Writing – review & editing.

Declaration of Competing Interest

The authors declare that they have no known competing financial interests or personal relationships that could have apeared to influence the work reported in this paper.

Data availability

Data will be made available on request.

Acknowledgements

The authors wish to thank the Basque Government and the University of the Basque Country UPV/EHU as the source of our main financial support: GIA consolidated Research Groups (https://www.ehu.eus/es/web/gia) IT1057-16 (GIC15/152) and GIU13/03. These financing bodies have played an exclusively economic role in the study.

Appendix A

DATE	youtube web page	Content	EIS reference selection
27 June 2012	https://youtu.be/GntXhA-5t7g	Wind on beaches	YES
28 June 2014	https://youtu.be/L9HrgL753I8	Wind and waves in a sailing boat	YES
04 June 2015	https://youtu.be/9mNB9QyMMzU	Wind on beaches (erroneous dated on 05 june 2015)	YES
03 July 2015	https://youtu.be/zrnKXcslZCs	Wind on beaches	YES
10 July 2015	https://youtu.be/5500QUTFi1M	Wind on beaches	YES
10 July 2015	https://youtu.be/6qDw9EDAoBY	Wind on beaches	YES
10 July 2015	https://youtu.be/gvgxU5sqO-E	Airplain landing in San Sebastian	YES
27 August 2016	https://youtu.be/eDQdgRsJlFw	Wind on beaches	NO ($V_{1h} < 50$ km h^{-1})
13 Sept 2016	https://youtu.be/DHTlEMCX0L8	Wind on beaches	YES
14 August 2017	https://youtu.be/Ue-rlTcTkl0	Wind on beaches	NO ($V_{1h} < 50$ km h^{-1})
09 January 2020	https://youtu.be/nCkx5Caj28w	Landscape near the coast in Bilbao	NO ($Fr_m > 1$)
04 May 2020	https://youtu.be/j9manxW_NeE	Wind on coastal promenade. Tree falling in Bilbao city	YES

References

AEMET, 2016. Agencia Estatal de Meteorología. Aemetblog [In Spanish]. https://aemetblog.es/2016/09/07/las-galernas/ (accessed 06 July 2022).

AEMET, 2018. Agencia Estatal de Meteorología. Aemetblog, Arteche, J.L. [In Spanish]. https://aemetblog.es/2018/04/20/la-galerna-del-cantabrico/ (accessed 06 July 2022).

Alonso, L.A., Gangoiti, G., Navazo, M., Maruri, M., Garcia, J.A., Aranda, J.A., 1998. The Punta Galea boundary layer profiler: Intercomparison with radiosonde data and first mesoscale meteorological case studies. Meteorol. Z. 7 (5), 203–212. https://doi.org/10.1127/metz/7/1998/203.

Aranda, J.A., Mader, J., 2012. Galernas, ¿Estamos preparados? [In Spanish]. https://www.slideshare.net/aztitecnalia/galernas-estamos-preparados (accessed 06 July 2022).

Arasti, E., 1999. La galerna típica [In Spanish]. https://repositorio.aemet.es/handle/20.500.11765/1797 (accessed 06 July 2022).

Arasti, E., 2001. La galerna Típica: una perturbación atrapada en la costa. In: Proceedings of the 5th National Symposium of Meteorological Forecasting. Madrid, Nov 2001 [In Spanish]. https://repositorio.aemet.es/handle/20.500.11765/4698 (accessed 06 July 2022).

Australian Government Bureau of Meteorology, 2011. The Big Bust—Southerly Busters Explained. https://media.bom.gov.au/social/blog/18/the-big-bustsou (accessed 06 July 2022).

Bell, W., Hersbach, H., Berrisford, P., Horányi, A., Muñoz-Sabater, J., Nicolas, J., Radu, R., Schepers, D., Simmons, A., Soci, C., 2020. Satellite observations in support of the Copernicus Climate Change Service. In: Proceedings Volume 11527, Space, Satellites, and Sustainability; 115270C (2020). https://doi.org/10.1117/12.2576497.

Berry, G., Jakob, C., Reeder, M., 2011. Recent global trends in atmospheric fronts. Geophys. Res. Lett. 38 (L21812), 1–6. https://doi.org/10.1029/2011GL049481.

Bitsa, E., Flocas, H., Kouroutzoglou, J., Hatzaki, M., Rudeva, I., Simmonds, I., 2019. Development of a Front Identification Scheme for Compiling a Cold Front Climatology of the Mediterranean. Climate. 7 (11), 130. https://doi.org/10.3390/cli7110130.

Casado, J.L., 2005. Naufragios en los litorales de Cantabria, in: Cantabria Infinita. 3, 43-53 [In Spanish]. https://www.divulgameteo.es/ampliab/4/718/Naufragios-en-los-litorales-de-Cantabria.html.

Colquhoun, J.R., Shepherd, D.J., Coulman, C.E., Smith, R.K., McInnes, K., 1985. The Southerly Burster of South Eastern Australia: an Orographically Forced Cold Front. Mon. Weather Rev. 113 (12), 2090–2107. https://journals.ametsoc.org/view/journals/mwre/113/12/1520-0493_1985_113_2090_tsbose_2_0_co_2.xml.

Copernicus Climate Change Service, 2018. ERA5: Fifth generation of ECMWF atmospheric reanalyses of the global climate. Copernicus Climate Change Service (C3S) Climate Data Store (CDS). https://cds.climate.copernicus.eu/cdsapp#!/dataset/reanalysis-era5-pressure-levels?tab=overview (accessed 06 July 2022).

Doty, B.E., Kinter III, J.L., 1995. Geophysical Data Analysis and Visualization Using the Grid Analysis and Display System. National Aeronautics and Space Administration, Washington, DC (United States). https://ntrs.nasa.gov/citations/19960022591.

EUMETRAIN, 2012. International training project sponsored by EUMESAT. http://eumetrain.org/satmanu/CM4SH/Australia/ShCF/print.htm (accessed 06 July 2022).

Gangoiti, G., 2002. Diagnosis and Analysis of severe weather episodes in the Basque Country. https://addi.ehu.es/handle/10810/55032 (accessed 06 July 2022).

Gangoiti, G., 2003. Identification of "Galerna" events in the regional meteorological network of the Basque Country: a selection of 7 events in 2002. https://addi.ehu.es/handle/10810/55085 (accessed 06 July 2022).

Gangoiti, G., Pérez-Landa, G., Alonso, L., Maruri, M., Navazo, M., 2000. Episodes of persistent wind shear over the Bay of Biscay. In: Proceedings of the 9th International Workshop on Technical and Scientific Aspects of MST Radar and COST 76 Final Profiler Workshop, Toulouse, France-March 13–18, SCOSTEP and Météo France, 295–299. https://www.researchgate.net/publication/361810378_Episodes_of_persistent_wind_shear_over_the_Bay_of_Biscay (accessed 06 July 2022).

Gangoiti, G., Millán, M.M., Salvador, R., Mantilla, E., 2001. Long-range transport and re-circulation of pollutants in the western Mediterranean during the project Regional Cycles of Air Pollution in the West-Central Mediterranean Area. Atmos. Environ. 35 (36), 6267–6276. https://doi.org/10.1016/S1352-2310(01)00440-X.

Gangoiti, G., Alonso, L., Maruri, M., Navazo, M., Pérez-Landa, G., 2002. UHF Radar detection and numerical simulation of an episode of foehn and lee waves over the northern coast of Iberia. J. Appl. Meteorol. 41, 230–240. https://doi.org/10.1175/1520-0450(2002)041<0230:URDANS>2.0.CO;2.

Gangoiti, G., Rodríguez-García, A., Sáez de Cámara, E., Torre-Pascual, E., Gómez, M.C., de Blas, M., García, J.A., García-Ruiz, E., Zuazo, I., Valdenebro, V., Iza, J., 2022a. Revealed frontogenesis of Galernas in the Bay of Biscay. Zenodo. https://doi.org/10.5281/zenodo.6832275.

Gangoiti, G., Rodríguez-García, A., Sáez de Cámara, E., Torre-Pascual, E., Gómez, M.C., de Blas, M., García, J.A., García-Ruiz, E., Zuazo, I., Valdenebro, V., Iza, J., 2022b. Revealed frontogenesis of Galernas in the Bay of Biscay: frontal identification system (FIS) wind thresholds test. Zenodo. https://doi.org/10.5281/zenodo.7133368.

Gaztelumendi, S., Egaña, J., Ruiz, M., Pierna, D., Otxoa de Alda, K., Gelpi, I.R., 2011. An analysis of Cantabric coastal trapped disturbances. In: Proceedings of the Sixth International Conference on EuroGOOS 4–6 October, Sopot, Poland. In: https://eurogoos.eu/download/conference_proceedings/EuroGOOS6thConf_proceedings.pdf.

Gill, A.E., 1977. Coastally trapped waves in the atmosphere. Q. J. R. Meteorol. Soc. 103, 431–440. https://doi.org/10.1002/qj.49710343704.

González, S., Callado, A., Werner, E., Escribà, P., Bech, J., 2018. Coastally trapped disturbances caused by the tramontane wind on the northwestern Mediterranean: numerical study and sensitivity to short-wave radiation. Q. J. R. Meteorol. *Soc*. 144 (714), 1321–1336. https://doi.org/10.1002/qj.3320.

Hersbach, H., Bell, B., Berrisford, P., Hirahara, S., Horányi, A., Muñoz-Sabater, J., Nicolas, J., Peubey, C., Radu, R., Schepers, D., Simmons, A., Soci, C., Abdalla, S., Abellan, X., Balsamo, G., Bechtold, P., Biavati, G., Bidlot, J., Bonavita, M., De Chiara, G., Dahlgren, P., Dee, D., Diamantakis, M., Dragani, R., Flemming, J., Forbes, R., Fuentes, M., Geer, A., Haimberger, L., Healy, S., Hogan, R.J., Hólm, E., Janisková, M., Keeley, S., Laloyaux, P., Lopez, P., Lupu, C., Radnoti, G., de Rosnay, P., Rozum, I., Vamborg, F., Villaume, S., Thépaut, J.-N., 2020. The ERA5 global reanalysis. Q. J. R. Meteorol. Soc. 146, 1999–2049. https://doi.org/10.1002/qj.3803.

Hewson, T.D., 1998. Objective fronts. Meteorol. Appl. 5, 37–65. https://doi.org/10.1017/S135048279800055.

Knapp, K.R., 2008. Scientific data stewardship of International Satellite Cloud Climatology project B1 global geostationary observations. J. Appl. Remote. Sens. 2 (1), 023548 https://doi.org/10.1117/1.3043461.

Liria, P., Aranda, J.A., 2013. Galernas: predicción y seguimiento [In Spanish]. https://issuu.com/aztitecnalia/docs/galernas_prediccion_y_seguimiento (accessed 06 July 2022).

Mass, C.F., Albright, M.D., 1987. Coastal Southerlies and Alongshore Surges of the West Coast of North America: evidence of Mesoscale Topographically Trapped Response to Synoptic Forcing. Mon. Weather Rev. 115 (8), 1707–1738. https://journals.ametsoc.org/view/journals/mwre/115/8/1520-0493_1987_115_1707_csaaso_2_0_co_2.xml.

Millán, M.M., Salvador, R., Mantilla, E., Kallos, G., 1997. Photooxidant dynamics in the Mediterranean basin in summer: results from European research projects. J. Geophys. Res. 102 (D7), 8811–8823. https://doi.org/10.1029/96JD03610.

National Research Council, 1992. Coastal Meteorology: A Review of the State of the Science. The National Academies Press, Washington, DC. https://doi.org/10.17226/1991.

Nuss, W.A., Bane, J.M., Thompson, W.T., Holt, T., Dorman, C.E., Ralph, F.M., Rotunno, R., Klemp, J.B., Skamarock, W.C., Samelson, R.M., Rogerson, A.M., Reason, C., Jackson, P., 2000. Coastally Trapped Wind Reversals: Progress toward Understanding. Bull. Am. Meteorol. Soc. 81 (4), 719–744. https://doi.org/10.1175/1520-0477(2000)081<0719:CTWRPT>2.3.CO;2.

Parish, T.R., Rahn, D.A., Leon, D., 2015. Aircraft Observations and Numerical Simulations of the developing stage of a Southerly Surge near Southern California. Mon. Weather Rev. 143 (12), 4883–4903. https://journals.ametsoc.org/view/journals/mwre/143/12/mwr-d-15-0140.1.xml.

Rahn, D.A., Parish, T.R., 2008. A Study of the Forcing of the 22–25 June 2006 Coastally Trapped Wind Reversal based on Numerical Simulations and Aircraft Observations. Mon. Weather Rev. 136 (12), 4687–4708. https://journals.ametsoc.org/view/journals/mwre/136/12/2008mwr2361.1.xml.

Reason, C.J.C., Jury, M.R., 1990. On the generation and propagation of the southern African coastal low. Q. J. R. Meteorol. Soc. 116, 1133–1151. https://rmets.onlinelibrary.wiley.com/doi/abs/10.1002/qj.49711649507.

Reason, C.J.C., Steyn, D.G., 1990. Coastally trapped disturbances in the lower atmosphere: dynamic commonalities and geographic diversity. Prog. Phys. Geogr. 14 (2), 178–198. https://doi.org/10.1177/030913339001400202.

Reid, H.J., Leslie, L.M., 1999. Modeling coastally trapped wind surges over southeastern Australia. Part I: timing and speed of propagation. Weather Forecast. 14 (1), 53–66. https://doi.org/10.1175/1520-0434(1999)014<0053:MCTWSO>2.0.CO;2.

Saha, S., Moorthi, S., Wu, X., Wang, J., Nadiga, S., Tripp, P., Behringer, D., Hou, Y.-T., Chuang, H.-Y., Iredell, M., Ek, M., Meng, J., Yang, R., Mendez, M.P., Van Den Dool, H., Zhang, Q., Wang, W., Chen, M., Becker, E., 2014. The NCEP climate forecast system version 2. J. Clim. 27 (6), 2185–2208. https://journals.ametsoc.org/view/journals/clim/27/6/jcli-d-12-00823.1.xml.

Schemm, S., Rudeva, I., Simmonds, I., 2015. Extratropical fronts in the lower troposphere–global perspectives obtained from two automated methods. Q. J. R. Meteorol. Soc. 141, 1686–1698. https://doi.org/10.1002/qj.2471.

Simmonds, I., Keay, K., Tristram Bye, J.A., 2012. Identification and Climatology of Southern Hemisphere Mobile Fronts in a Modern Reanalysis. J. Clim. 25 (6), 1945–1962. https://journals.ametsoc.org/view/journals/clim/25/6/jcli-d-11-00100.1.xml.

Wang, S., Leslie, L., Ray, T., Speer, M., Kuleshov, Y., 2020. Analysis of a southerly buster event and associated solitary waves. J. South. Hemisphere Earth Syst. Sci. 69, 205–215. https://doi.org/10.1071/ES19015.